Simulation of cell rolling and adhesion on surfaces in shear flow: general results and analysis of selectin-mediated neutrophil adhesion

Daniel A. Hammer and Sachin M. Apte
School of Chemical Engineering, Cornell University, Ithaca, New York 14853

ABSTRACT The receptor-mediated adhesion of cells to ligand-coated surfaces in viscous shear flow is an important step in many physiological processes, such as the neutrophil-mediated inflammatory response, lymphocyte homing, and tumor cell metastasis. This paper describes a calculational method which simulates the interaction of a single cell with a ligand-coated surface under flow. The cell is idealized as a microvilli-coated hard sphere covered with adhesive springs. The distribution of microvilli on the cell surface, the distribution of receptors on microvilli tips, and the forward and reverse reaction between receptor and ligand are all simulated using random number sampling of appropriate probability functions. The velocity of the cell at each time step in the simulation results from a balance of hydrodynamic, colloidal and bonding forces; the bonding force is derived by summing the individual contributions of each receptor-ligand tether. The model can simulate the effect of many parameters on adhesion, such as the number of receptors on microvilli tips, the density of ligand, the rates of reaction between receptor and ligand, the stiffness of the resulting receptor-ligand springs, the response of springs to strain, and the magnitude of the bulk hydrodynamic stresses. The model can successfully recreate the entire range of expected and observed adhesive phenomena, from completely unencumbered motion, to rolling, to transient attachment, to firm adhesion. Also, the method can generate meaningful statistical measures of adhesion, including the mean and variance in velocity, rate constants for cell attachment and detachment, and the frequency of adhesion.

We find a critical modulating parameter of adhesion is the fractional spring slippage, which relates the strain of a bond to its rate of breakage; the higher the slippage, the faster the breakage for the same strain. Our analysis of neutrophil adhesive behavior on selectin-coated (CD62-coated) surfaces in viscous shear flow reported by Lawrence and Springer (Lawrence, M. B., and T. A. Springer. 1991. *Cell.* 65:859–874) shows the fractional spring slippage of the CD62-LECAM-1 bond is likely below 0.01. We conclude the unique ability of this selectin bond to cause neutrophil rolling under flow is a result of its unique response to strain. Furthermore, our model can successfully recreate data on neutrophil rolling as a function of CD62 surface density.

INTRODUCTION

The adhesion of cells to surfaces under conditions of flow is a principal step in the neutrophil-mediated inflammatory response (Harlan, 1975), lymphocyte trafficking (Butcher et al., 1980), and disease processes such as cancer cell metastasis (Pauli et al., 1990; Rice and Bevilacqua, 1989). A great deal of research in molecular biology now concerns itself with how adhesion in each of these processes is regulated at the molecular level.

For example, adhesion in the neutrophil-mediated inflammatory response has received considerable attention recently (Lawrence et al., 1990; Lawrence and Springer, 1991; von Adrian et al., 1991; Ley et al., 1991). In inflammation, neutrophils, when presented with a region of tissue under infiltration from a foreign invader, will adhere to the endothelial cells lining blood vessels adjacent to the infected tissue space, in a process called margination (Atherton and Born, 1972, 1973; Harlan, 1975). After adhesion, the neutrophils undergo morphological changes, employ proteases to break down the interendothelial connections and basement membrane, and crawl into the tissue space to phagocytose invaders (Harlan, 1975). The accumulation of neutrophils at the proper site requires local regulation of neutrophil adhesion.

It is known that neutrophils possess many adhesion molecules (Lawrence and Springer, 1991; Springer, 1990), and it is suspected that local neutrophil accumulation is regulated by the concerted action of different sets of neutrophil-endothelial adhesion molecules such as LFA-1/ICAM-1 or ICAM-2, and LECAM-1/CD62 (or other selectins) (Lawrence and Springer, 1991; Springer, 1990; von Adrian et al., 1991). Excellent experimental work on determining which of these molecular pairs might be responsible for neutrophil margination and arrest in the microvasculature under flow has recently been performed by several groups (Lawrence et al., 1990; Lawrence and Springer, 1991; von Adrian et al., 1991; Ley et al., 1991). In these studies, either parallel-plate flow chambers, to generate shear stresses found in the post capillary venules (1–4 dynes/cm^2) (Lawrence et al., 1990; Lawrence and Springer, 1991), or direct intravital observation (von Adrian et al., 1991; Ley et al., 1991) were used to observe neutrophil adhesive phenomena. From these studies, it has been shown CD62/LECAM-1 binding promotes the initial rolling and adhesion of neutrophils on endothelia, and LFA-1/ICAM-1 binding strengthens the adhesion, promoting arrest and extravasation (Lawrence and Springer, 1991; von Adrian et al., 1991; Ley et al., 1991). Understanding the structural and functional characteristics of the CD62/LECAM-1 pair which make it well suited to cause adhesion in flow will help elucidate how adhesion in flow is regulated at the molecular level for neutrophils, and will likely provide clues as to how lymphocytes and metastasizing tumor cells regulate their adhesion as well.

A mathematical formalism which can explain cell adhesion under flow would be of great help in quantifying

Address correspondence to Dr. Hammer.

0006-3495/92/07/035/23 $2.00

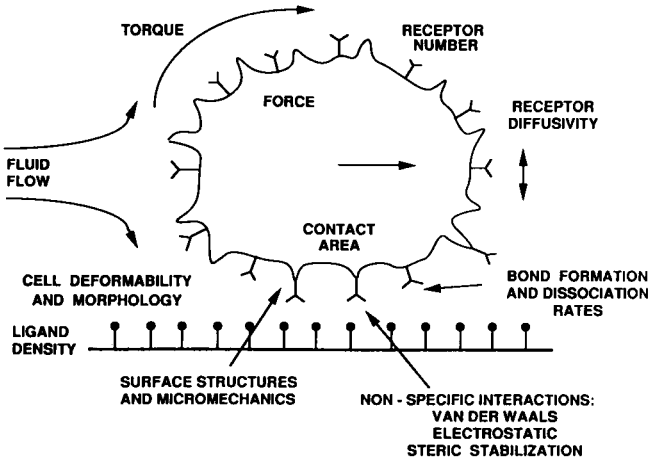

FIGURE 1 Many chemical and physical factors are suspected of playing a role in receptor-mediated cell adhesion to ligand-coated surfaces. Among the chemical factors are the numbers of receptors, the density of ligand on the substrate, and the rates of reaction between them (as well as their affinity for each other). Receptor diffusivity contributes to the rate of reaction in diffusion-limited binding, and provides an upper limit outside the diffusion limit. These chemical factors determine the number of macromolecular tethers formed during collision. Physical factors which affect the outcome of the interaction include the magnitude of fluid forces and torques acting on the cell, which must be countered by the bonds in the interface; colloidal interactions, which result in additional forces which affect the local and global motion of the cell near the surface; the bulk deformability of the cell as a whole, which indicates how externally applied stresses are transmitted to the cell-substrate interface; and microstructure and micromechanics, which determines which receptors are close enough to bind the surfaces, and relates to the forces acting on tethers to their rates of formation and breakage. The net motion of the cell is a result of a net force imparted on the cell by these chemical and physical forces.

the relationship between molecular properties of adhesion molecules and adhesion itself. Referring to Fig. 1, one would ultimately like to describe how a cell which possesses a certain number of receptors interacts with a surface of known ligand density, when subjected to an imposed shear stress. Important factors in such a description are rates of reaction and affinity between receptor and ligand, the morphology of the cell surface, colloidal interactions between the cell and surface, and mechanical properties of the bonds, such as their strength and response to strain. The objective of such a calculation would be to describe the translational and angular velocities of the cell on the surface as various parameters which describe these factors are altered.

Our primary objective is to define regions in parameter space where one could recreate experimental observations of cell motion on surfaces, for example, observations of neutrophil rolling on CD62 surfaces (Lawrence and Springer, 1991), to determine what must be true about the CD62/LECAM-1 interaction for it to be a potent promoter of neutrophil rolling and arrest. An additional objective is to develop a method that is sufficiently robust to describe the wide range of adhesive phenomena reported for the motion of cells on surfaces. Of principal interest is "start-stop" type phenomena (Cozens-Roberts et al., 1990*c*; Doroszewski, 1980; Lawrence and Springer, 1991; Schmid-Schönbein et al., 1987; Tempelman and Hammer, 1990; Tissot et al., 1991; Wattenbarger et al., 1990; House and Lipowsky, 1991), in which the cell moves in an erratic fashion (fluctuating velocity) over the surface. We assume these fluctuations in velocity are due to fluctuations in binding between receptor and ligand. To characterize these fluctuations, we perform a simulation of cell motion on a surface, where the trajectory of each cell is followed independently and dynamically, and where the molecular binding, while still determined in principle by intrinsic characteristics of the adhesion molecules, is also determined by random statistical sampling of a probability distributions which describe the binding (or unbinding) of a particular molecular pair.

Hopefully, such a model would characterize all types of cell motion of surfaces under flow, including rolling, tumbling, transient adhesion, and complete attachment. Although separate groups have calculated the rolling velocity (Dembo et al., 1988; Schmid-Schönbein et al., 1987), or used probabilistic/statistical methods to analyze adhesion or detachment (Cozens-Roberts et al., 1990*b, c*), no group has yet to combine these approaches. Hammer and Lauffenburger (Hammer and Lauffenburger, 1987) used a deterministic, phase plane analysis to determine whether cells would adhere to a surface in shear flow after an initial collision, thus, restricting themselves to two types of interaction: arrest, and all others. Cozens-Roberts and co-workers extended this work using a probabilistic description of receptor-ligand binding which allowed for a homogeneous population to be described by a continuous distribution of bound states, simultaneously allowing one fraction to be unbound, and another fraction to be bound (Cozens-Roberts et al., 1990*b*). Once again, no attempt was made to distinguish between unbound states. Although this work correctly rendered the force and torque externally applied by the fluid on the cell (assuming the cell was a sphere), it assumed for simplicity stresses were uniformly distributed over bonds in the cell-substrate interface, which led to the conclusion that a single tether, regardless of where placed in the cell-substrate interface, can keep a cell adherent. This is likely not the case, since Evans and others have shown, in a derivation of the critical tension necessary to peel a membrane, that receptors most responsible for retarding the peeling of the membrane are those within a small critical distance of the cell's back edge (Dembo et al., 1988; Evans, 1985*a, b*; Tözeren, 1990). Dembo and co-workers (Dembo et al., 1988) extended Evans' work to determine the rate at which a one dimensional membrane of infinite extent would peel if exposed to a tension above the critical ten-

sion. Although an attempt was made to relate hydrodynamic stresses to membrane tensions in this calculation, the details of known hydrodynamic solutions for particle motion near a wall were not included (Dembo et al., 1988). Furthermore, the membrane in the cell substrate interface was assumed to be smooth, whereas upon initial contact, leukocytes are known to be ruffled and coated with numerous surface asperities (Bongrand and Bell, 1984; Knutton et al., 1975; Loor and Hagg, 1975; Picker et al., 1991; Evans and Yeung, 1989; Yeung and Evans, 1989). Also, this was a deterministic analysis which did not characterize the effect of fluctuations in binding on the rate of peeling. Finally, because the interface was assumed to be infinite in extent, binding deep within the interface was assumed to be at equilibrium. Because the contact area is finite in extent, significant binding will only occur if the time scale for reaction is smaller than the time scale for transit of a receptor through the interface. If this is not the case, binding within the interface would not be at equilibrium, and the extent of binding would be greatly reduced.

This paper improves upon these previous works by retaining the detailed description of hydrodynamic forces for a particle near a wall (Hammer and Lauffenburger, 1987; Cozens-Roberts et al., 1990*a, b;* Goldman et al., 1967*a, b*) while, through simulation, characterizing the statistical fluctuations of receptor-ligand binding. Because the stress imparted by a bond will depend on its length, orientation, and position within the cell-substrate interface, our method will lead naturally to a realistic description of the spatial distribution of stresses in the interface. The cell is modeled as a rough body, and the interface assumed to be finite in extent, corrections we feel are essential to properly describe dynamic, initial leukocyte adhesion.

Using this method, we determine how the mean and variance of the instantaneous particle velocity, as well as other statistical measures of adhesion we will soon introduce, are affected by properties of the receptor macromolecules, surface microstructure, and binding characteristics between receptor and ligand. Our model can describe the wide spectrum of adhesive phenomena observed in experiments, from rolling, to transient adhesion, to firm attachment. In addition, the simulations allow us to make very specific conclusions about the nature of the CD62-LECAM-1 bond which allows it to mediate neurophil rolling.

MODEL FORMULATION

The model geometry and coordinate system are shown in Fig. 2. A sphere of radius R_c is covered by N_{mv} microvilli of radius R_{mv} and length L_{mv}. The microvilli are assumed to be rigid, oriented normal to the surface, and randomly distributed about the cell surface. For all cases in which hydrodynamic functions based on the size of the particles are needed, we use an effective hydrodynamic radius, defined $R_{ch} = R_c + L_{mv}$. There are R_T receptors of a given type on the cell, also randomly distributed. We assume the surface has a ligand density of N_l molecules.

We assume the adhesion molecules are springs. The force a molecule exerts on the cell will depend on the (x, y, z) coordinates of the molecule on both the microvillus $\vec{x}_m = (x_m, y_m, z_m)$ and on the substrate $\vec{x}_o = (x_o, y_o, z_o)$. Due to the translation and rotation of the cell, the vectors $\vec{x}_m$ and $\vec{x}_o$ change with time (see Appendix 1), and one can describe each bond by a time-varying vector $\vec{x}_b = \vec{x}_o - \vec{x}_m$.

To determine the reaction between receptor and ligand, we use kinetic rate expressions, appropriate for the model of an adhesion molecule as a spring (Dembo et al., 1988), which relate the forward reaction rate k_f, and the reverse reaction rate, k_r, to the separation distance x_m between the microvillus tip and the surface,

$$k_f = k_f^o \exp\left(-\frac{\sigma_{ts}(x_m - \lambda)^2}{2k_bT}\right) \quad (1)$$

$$k_r = k_r^o \exp\left(\frac{(\sigma - \sigma_{ts})(x_m - \lambda)^2}{2k_bT}\right), \quad (2)$$

where λ is the equilibrium separation distance for the spring, k_bT is the thermal energy (product of the Boltzmann constant and temperature), σ is the spring constant, σ_{ts} is the transition state spring constant, and the superscript "o" refers to reaction rates which occur at the spring's equilibrium length. These expressions, first used by Dembo and co-workers (Dembo et al., 1988) assure that, through microscopic reversibility, the ratio k_f/k_r at any separation distance is given:

$$\frac{k_f}{k_r} = \frac{k_f^o}{k_r^o} \exp\left(-\frac{\sigma(x_m - \lambda)^2}{2k_bT}\right). \quad (3)$$

Eq. 3 states that at equilibrium, the likelihood of finding a molecular pair is reduced as the separation deviates from equilibrium. Likewise, Eq. 1 indicates the ability of the forward reaction to proceed at separations different than the equilibrium separation is also reduced. In the limit $\sigma_{ts} = 0$, the forward reaction would proceed at the same rate regardless of separation, which leads to the awkward conclusion that molecules separated by an infinite distance might actually react. In contrast, an infinite value for σ_{ts} suggests the reaction might only proceed when the separation is exactly equal to the spring's equilibrium length; this is also an unrealistic limit, for we would expect some extent of reaction for minor perturbations in separation around the equilibrium length. Therefore, it seems physically realistic to expect σ_{ts} to be finite and nonzero.

Eqs. 1 and 3 give rise to an exceedingly interesting expression for the reverse reaction rate with enormous

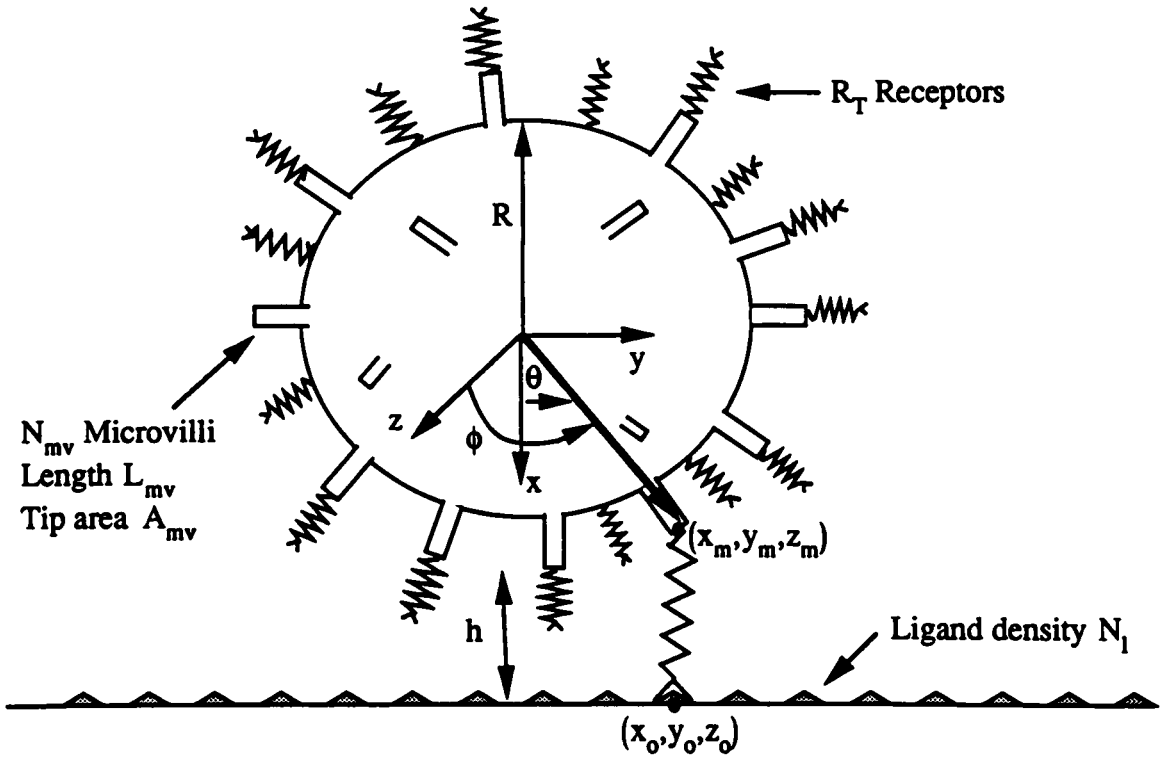

FIGURE 2 In our microvilli-coated hard sphere idealization of a cell's interaction with a surface, we model the cell as a hard sphere of radius R_c, covered with N_{mv} microvilli of length L_{mv} and tip area A_{mv}. R_T receptors are randomly distributed over the cell surface, and the density of ligand on the substrate is assumed to be N_l. One can monitor the positions of all species in the problem with a cartesian coordinate system whose origin is at the cell's center. Also, the spherical coordinates θ and φ can be used as an alternative indicator of microvilli or receptor positions on the cell surface. The position of the end of each macromolecular tether attached to the microvillus is given by the vector (x_m, y_m, z_m); likewise, its position on the substrate is given (x_o, y_o, z_o). The distance h is a time varying quantity that monitors the separation distance between the body, which has an effective radius $R_{ch} = R_c + L_{mv}$, and the surface.

implications for adhesion. Examining Eq. 2, one sees that whether the rate of bond breakage (k_r) increases with extension depends on the sign of $\sigma - \sigma_{ts}$. Should $\sigma - \sigma_{ts}$ be positive, bond extension will lead to an accelerated rate of breakage, previously termed "slip bonds" (Dembo et al., 1988). Should $\sigma - \sigma_{ts}$ be negative, bond extension will actually reduce the rate of breakage, a limit called "catch bonds," which have been likened to a finger prison (Dembo et al., 1988). Should it be without sign, one could consider these "ideal bonds," which break at the same rate regardless of extension (Dembo et al., 1988). We shall show the magnitude of $\sigma - \sigma_{ts}$ has a large effect on adhesion of cells under conditions of flow.

When considering the amount of binding which can occur between cell and surface, it is reasonable to ask how many receptors are available for binding, considering the roughness of the cell surface. Because microvilli lengths are much longer than the lengths of receptors themselves (Bongrand and Bell, 1984), it is reasonable to assume only those receptors at the tips of microvilli have anything to do with initial adhesion. When one considers that the tip of a microvillus is $\sim 10^{-2}$ μm^2 (Bongrand and Bell, 1984), the net surface area of a leukocytes is from 400 to 500 μm^2 (Evans and Yeung, 1989; Yeung and Evans, 1989), and the number of adhesion molecules can be 5×10^4 or lower (eg., 2×10^4 LECAM-1 molecules/neutrophil; Lawrence and Springer, 1991), the mean number of receptors per microvillus can easily be one or fewer. The number of uniformily distributed receptors on tips of microvilli is given by the discrete Poisson probability distribution for finding n receptors on the tip of a single microvillus,

$$P(n) = \frac{\left(\frac{R_T A_{mv}}{A_c}\right)^n \exp\left(-\frac{R_T A_{mv}}{A_c}\right)}{n!}, \qquad (4)$$

where $R_T A_{mv}/A_c$ is the average number of receptors on a microvillus tip. Appendix 1 outlines how the number of receptors on each microvillus is calculated from this distribution.

If a microvillus tip is a given distance x_m from the substrate, the kinetic rates of forward reaction is given by Eq. 1. The reverse reaction rate is based on the length of the spring, $|\vec{x}_b|$, which replaces x_m in Eq. 2. From these, probabilities for the forward and reverse reaction between receptor and ligand in a given time step Δt can be calculated and sampled, as described in Appendix 1.

Each existing bond is characterized by the vector $\vec{x}_b$, and the force imparted by the spring on the cell is

$$\vec{F}_b = \sigma(|\vec{x}_b| - \lambda)\hat{i}_b, \quad (5)$$

which can be resolved in each direction, and the associated torques can also be calculated (Appendix 1). The forces and torques due to the adhesion molecules acting on the cell will, in combination with the hydrodynamic and colloidal forces acting on the particle, give rise to a net motion. It is well known that colloidal forces exist between biological surfaces, some of which are similar to those seen between inert, nonbiological particles, and some of which are unique to biological bodies (Israelachvili, 1985). Details of calculating the colloidal interactions are in Appendix 2.

Once all the forces on the cell are known at each time step, the calculation of the velocities is performed using specific hydrodynamic functions which relate the applied forces and torques to the six components of translation and rotation (Brenner, 1961; Goldman et al., 1967*a,b;* Jeffrey, 1915). The relationship between externally applied forces and torques and motions is written

$$\vec{U} = M\vec{F}, \quad (6)$$

where

$$\vec{U} = (V_x, V_y, V_z, \Omega_x, \Omega_y, \Omega_z) \quad (7)$$

$$\vec{F} = (F_x^b + F_x^c, F_y^b + F^s, F_z^b, C_x^b, C_y^b, C_z^b + C_z^s), \quad (8)$$

and M is the mobility matrix containing the previously referenced hydrodynamic functions which depend on the separation distance between cell and surface, the hydrodynamic cell radius R_{ch}, and solution viscosity, μ. In Eqs. 7 and 8, subscripts indicate direction, and superscripts "b", "c" and "s" indicate forces due to bonding, colloidal forces and shear, respectively. Inertia is not a factor in the force balance, because the time scale for inertial interactions is quite short ($T_i = m/6\pi\mu R_{ch} = 10^{-5}$ s) due to the small mass and size of the cell, and the high viscosity of the medium. In each time step of the simulation, we calculate the extent of binding and the positions of all existing adhesive bonds, from which we can calculate the velocity of cell motion.

This serves as a brief outline of the method. Further details are given in the Appendices 1–3. Appendix 1 gives details of the method; Appendix 2 provides a method for calculating colloidal forces and provides further insight into the role of diffusion in reaction; and Appendix 3 provides a complete listing of the dimensionless parameters and dimensionless governing equations in this calculation. Dimensionless parameters are given in Table 1. These parameters will be reintroduced and defined in the results section as necessary.

TABLE 1 Dimensionless parameter values

Symbol	Definition	Values
α	Spring energy/fluid energy	10 to 300
ν	Spring energy/thermal energy	3×10^6 to 2×10^7
F_σ	Fractional spring slippage	−1 to 1
κ	Equilibrium constant	10^4 to 10^8
χ_o	Forward reaction rate/fluid flow rate	10^{-2} to 10^2
β_o	Reverse reaction rate/fluid flow rate	10^{-7} to 10^{-2}
N_{vdw}	van der Waals attraction/ fluid force	10^{-10} to 10^{-8}
N_{el}	Electrostatic interaction/ fluid force	10^8 to 10^{10}
N_{gr}	Gravitational force/ fluid force	10^{-5} to 10^{-3}
N_{ss}	Steric stabilization force/ fluid force	10^{-5} to 10^{-3}
δ_b	Bond length/cell radius	2×10^{-3} to 10^{-2}
δ_d^{-1}	Debye-Hückel length/cell radius	2×10^{-4} to 10^{-2}
δ_g	Glycocalyx length/cell radius	2×10^{-3} to 5×10^{-3}
δ_{mv}	Microvillus length/cell radius	10^{-2} to 5×10^{-1}
δ_1, δ_2	Ligand (receptor) length/ cell radius	10^{-3} to 2.5×10^{-3}
n_m	Number of receptors per microvillus	0.1 to 10

RESULTS

We can calculate the translational velocities $\tilde{V}_i$ and angular velocities $\tilde{\Omega}_i$ as a function of dimensionless time τ, but it would be cumbersome to present plots of such for all values of parameters used in this calculation. We seek more concise representations. One useful quantity is the mean velocity for a single cell, $\langle \tilde{V}_y \rangle$. In addition, the variance of the velocity, var $(\tilde{V}_y) = \langle (\tilde{V}(\tau) - \langle \tilde{V}(\tau) \rangle)^2 \rangle$ (in cases where the subscript in velocity is omitted, the y direction is implied), is an indication of the magnitude of the fluctuation in the velocity about its mean. These quantities can be determined for any individual cell during its trajectory across the surface. We always run the simulation sufficiently long so that our results for the averaged translational velocity or variance for a single cell are not functions of the simulation's duration.

Because each cell is unique, one can view each individual cell as a member of a population. If N cells are observed, then one may calculate the population mean and standard deviation for either the average velocity or the variance; the population mean will be indicated with an overbar: "—"; standard deviations in population-averaged quantities will be indicated with error bars on the simulation result. In most cases, we have found that $N = 10$ provides reasonable standard deviations which allow us to distinguish among population level results with confidence that the differences are due to true differences in the physics of binding, and not due to scatter among the population.

In Fig. 3, we show results from an example, illustrative simulation up to $\tau = 30$ for a set of parameters listed in the figure caption. The dimensionless parameters used in the calculation of this figure and Figs. 4–8 are derived

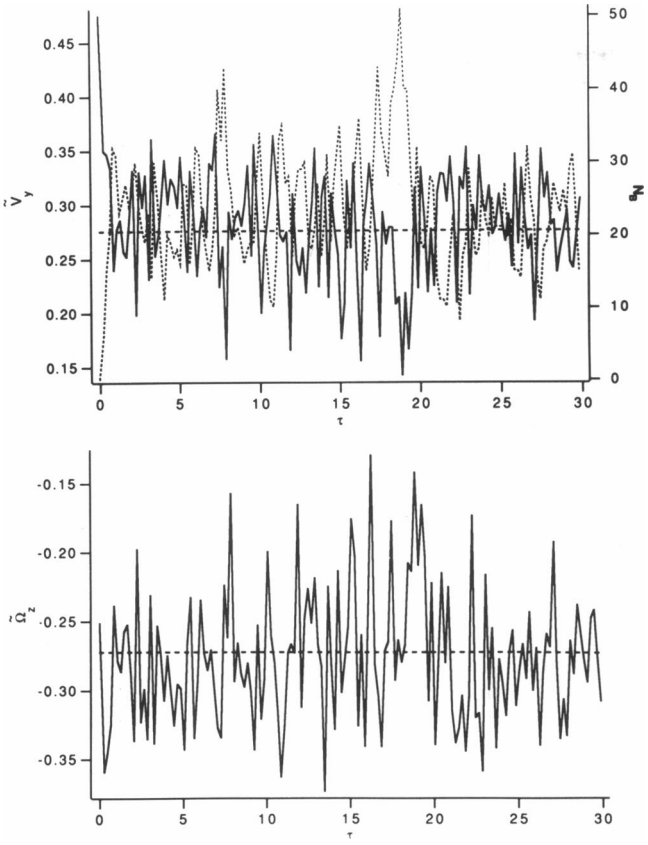

FIGURE 3 We plot the dimensionless instantaneous translational and angular velocities, and the number of bonds N_B, as a function of dimensionless time τ. (*A*) $\tilde{V}_y$ (*solid line*) and N_B (*dotted line*) as a function of τ. Importantly, there is an initial transient of approximately two time constants where the cell goes from a completely unencumbered state to a steadily bound state. $\langle \tilde{V}_y \rangle$ is 0.28. Note the number of bonds, N_B, is anticorrelated with the velocity; the slowest (fastest) motions of the cell are associated with the highest (lowest) number of bonds. (*B*) $\tilde{\Omega}_z$ as a function of τ. Note $\langle \tilde{\Omega}_z \rangle = -0.28$, which indicates that after an initial transient, the cell is rolling, because $\langle \tilde{\Omega}_z \rangle = -\langle \tilde{V}_y \rangle$. Parameter values for this simulation are $n_m = 5$, $F_\sigma = 0.1$, $N_{mv} = 6 \times 10^3$, $\kappa = 10^7$, $\alpha = 1.05 \times 10^2$, $\chi_o = 10$, $\beta_o = 10^{-6}$, $\nu = 5.95 \times 10^6$, $\delta_b = 3.95 \times 10^{-3}$, $N_{vdw} = 2 \times 10^{-9}$, $N_{el} = 2 \times 10^9$, $N_{ss} = 2 \times 10^{-4}$, $N_{gr} = 2 \times 10^{-2}$, $\delta_d^{-1} = 1.58 \times 10^{-4}$, $\delta_g = 3.95 \times 10^{-3}$, $\delta_l = \delta_2 = 1.97 \times 10^{-3}$, and $\delta_{mv} = 9.9 \times 10^{-3}$.

from the mean dimensional parameters listed in Table 2. The dimensionless velocities are scaled to a hydrodynamic velocity based on fluid shear rate at the wall, $\dot{\gamma}$ (see Appendix 3). The purpose of this figure is to illustrate features from the simulations which are common to all of the results of this paper, and not necessarily to understand the role of different parameter values on adhesion. All velocities fluctuate on a very short time scale, although we only show two components of the velocity vector $\tilde{\mathbf{U}}$ (Eq. 7). The notion of acceleration is not quite appropriate, because the time for change is infinitessimally short (equal to the inertial time scale) following a change in binding. Fig. 3 *A* gives the velocity in the direction of flow, $\tilde{V}_y$. In addition to $\tilde{V}_y$, we plot N_b, the number of bonds between the cell and surface at τ. At the beginning of the simulation, $\tilde{V}_y = 0.48$, the velocity of an unencumbered sphere near a surface at the initial separation of this simulation (Goldman et al., 1967*b*). Almost immediately after the initiation of binding, the cell begins to move on average more slowly over the surface, although on a short time scale the motion continues to fluctuate. This cell never becomes adherent, moving at its slowest $\tilde{V}_y = 0.15$, ~31% of its unencumbered velocity. Also, $\tilde{V}_y$ is inversely correlated to the amount of binding. Maxima in N_b yield minima in $\tilde{V}_y$, and the opposite is also true.

Fig. 3 *B* gives the angular velocity $\tilde{\Omega}_z$ of the cell normal to the direction of flow, and parallel to the substrate. The combination of $\tilde{V}_y$ and $\tilde{\Omega}_z$ allows us to address the question of whether the cell is translating faster than it is rotating. If translation exactly equals rotation

$$\tilde{V}_y = -\tilde{\Omega}_z. \tag{9}$$

If $\tilde{V}_y > -\tilde{\Omega}_z$, the cell is slipping; if $\tilde{V}_y < -\tilde{\Omega}_z$, it is spinning. The hydrodynamic solution for motion of an unencumbered sphere near a surface in simple shear predicts a substantial slip velocity (Goldman et al., 1967*b*). This can be seen at the onset this simulation, where $\tilde{V}_y = 0.48$ whereas $\tilde{\Omega}_z = -0.28$. Once a bond appears, it would be extended in the direction of flow as the cell translates faster than it rotates. This extension would generate a force which would act counter to the direction of flow (thus, slowing the particle's translation) and would generate a couple on the sphere which would enhance its rotation (increase rotation in the $-z$ direction). The net result, short of the bond disappearing, would be for the bond to apply exactly the correct force and couple to make the cell roll past it. This is indeed the case; should any bonds exist between the cell and surface, the cell will neither slip nor spin, as seen by the equality in magnitude in $\tilde{V}_y$ and $\tilde{\Omega}_z$ for all values of τ for which bonding exists, and the equality of $\langle \tilde{V}_y \rangle$ and $\langle -\tilde{\Omega}_y \rangle$, shown as dotted lines on these figures.

GENERAL RESULTS

We would like to examine general predictions of the model. In Fig. 4, we examine the effect of the number of receptors per microvillus, n_m, and number of microvilli (N_{mv}) on adhesion. An increase in the number of microvilli, or in the number of receptors per microvillus, decreases the population average velocity, $\langle \tilde{V}_y \rangle$. In these simulations, $F_\sigma = 0.1$, which indicates these bonds break more rapidly when under strain, but are relatively close to the ideal bond limit. Even with a microvilli surface coverage equal to roughly 6% of the cell surface (N_{mv} = 6,000), and on average 10 molecules per microvillus tip, the velocity is only 39% below its unencumbered value.

We provide representative traces of the velocity, for individual cells at each of three different receptor num-

TABLE 2 **Estimates for dimensional parameters of the model**

Parameter	Definition	Value range	Mean value	Neutrophil value	Source
R_c	Cell radius	2.5–50 μm	4.5 μm	3.75 μm	Lawrence and Springer, 1991; Evans and Yeung, 1989
L_{mv}	Microvillus length	0.2–2 μm	0.5 μm	0.5 μm	Bongrand and Bell, 1984
R_T	Receptor number	10^4–10^7	5×10^5	2×10^4	Lawrence and Springer, 1991
A_E	Excess area	2.0–3.0	2.5	2.1–2.2	Evans and Yeung, 1989
N_{mv}	Number of microvilli	500–10,000	6,000	500–8,000	Knutton et al., 1975; Loor and Hagg, 1975
N_l	Ligand density	10^9–10^{13} cm^{-2}	10^{11} cm^{-2}	2×10^{10} cm^{-2}	Lawrence and Springer, 1991
L_b	Bond length	5–50 nm	20 nm	50 nm	Springer, 1990
K	Affinity	10^{-7}–10^{-3} cm^2	10^{-5} cm^2	10^{-5} cm^2	Bell, 1981; Lawrence and Springer, 1991
k_f^o	Forward reaction rate	10^{-12}–10^{-7} cm^2/s	10^{-10} cm^2/s	6×10^{-9} cm^2/s	Hammer and Lauffenburger, 1987; Lawrence and Springer, 1991
μ	Viscosity	1–2 g/cm-s	1–2 g/cm-s	1 g/cm-s	Lawrence and Springer, 1991
$\dot{\gamma}$	Shear rate	50–400 s^{-1}	100 s^{-1}	180 s^{-1}	Lawrence and Springer, 1991
A_H	Hamaker constant	10^{-12} erg	10^{-12} erg	10^{-12} erg	Bongrand and Bell, 1984
N_i	Charge density	1 C/cm^3	1 C/cm^3	1 C/cm^3	Hammer and Lauffenburger, 1987; Bongrand and Bell, 1984
L_{dh}	Debye-Hückel length	8 Å	8 Å	8 Å	Bongrand and Bell, 1984
$\Delta\rho$	Density difference	0–0.1 g/cm^3	0.05 g/cm^3	0.05 g/cm^3	Bongrand and Bell, 1984
λ_{ss}	Steric constant	10^{-5}–10^{-3} dynes	10^{-5} dynes	10^{-5} dynes	Bongrand and Bell, 1984
σ	Spring constant	0.5–5 dyne/cm	1–2 dyne/cm	1–2 dyne/cm	Dembo et al., 1988; Evans et al., 1991
σ_{ts}	Transition state spring constant	−5–5 dyne/cm	0–2 dyne/cm	0–2 dyne/cm	Dembo et al., 1988
T	Temperature	277–310°K	310°K	298°K	Lawrence and Springer, 1991
L_1, L_2	Length of ligand and receptor layers	10–20 nm	10 nm	10 nm	Bell et al., 1984
L_g	Glycocalyx thickness	20–50 nm	20 nm	20 nm	Bell et al., 1984

bers from Fig. 4 *A* (n_m = 1, 5, and 10; N_{mv} = 6,000) (Fig. 4 *B–D*). When the receptor number is small (n_m = 1), the cell is not very adhesive, but because there are many opportunities for single binding events, the cell is often slowed by the binding. The variance is relatively high; var ($\tilde{V}_y$) = 1.9×10^{-3}. At n_m = 5, the variance goes through a minimum, var ($\tilde{V}_y$) = 6×10^{-4}. There are a fair number of receptors per microvillus tip which provide a constant, low level of binding sufficient to keep the cell rolling, but not enough to substantially lower the cell's rolling velocity. As the number of receptors is further increased (n_m = 10), the overall binding is greater (resulting in a lower rolling velocity), and occasionally a well-endowed microvillus with many receptors appears which has a large effect in retarding the velocity. Because there are sufficiently many of these microvilli, the variance in velocity increases (var ($\tilde{V}_y$) = 1.85×10^{-3}). Although we show complete data elsewhere (Hammer, 1992), there is often an identifiable minimum in the variance when the cells are rolling.

The two parameters which characterize the bond micromechanics are the fractional spring slippage, F_σ, which gives the fraction of the energy devoted to bond strain which is actually devoted to breaking the tethers, and α, the ratio of the spring constant to fluid energy (defined in Appendix 3). In Fig. 5, we plot the dependence of the population average rolling velocity on F_σ and α, in such a way that increasing values of α are representative of lower values of fluid shear rate, $\dot{\gamma}$. The dimensionless population average rolling velocity decreases as the shear rate decreases (with higher α). These changes in the dimensionless velocity with α are significant, because they indicate the role that chemistry plays in adhesion with respect to the flow; if the dimensionless rolling velocity were to remain constant as shear rate doubled, there would be a doubling in the velocity of the cell, because the velocity is scaled to the shear rate.

Decreases in the value of F_σ to lead to an increase in adhesiveness (Fig. 5). In these simulations, adhesion (V_y approaching 0) becomes significant at higher values of α when $F_\sigma \leq 0.05$, and becomes substantial when $F_\sigma \leq 0.01$ at all shear rates (values of α). It is clear that the response of bonds to strain is an extremely strong modulator of adhesion. Fig. 5, *B–D* shows examples of individual cell trajectories displaying a wide variety of different cell motions as both α and F_σ are altered. Fig. 5 *B* is an example of complete adhesion; Fig. 5 *C* of transient adhesion; and Fig. 5 *D* of tumbling, in which a cell never comes to rest, but displays large fluctuations in its velocity.

Fig. 5 shows lower F_σ or higher α leads to greater adhe-

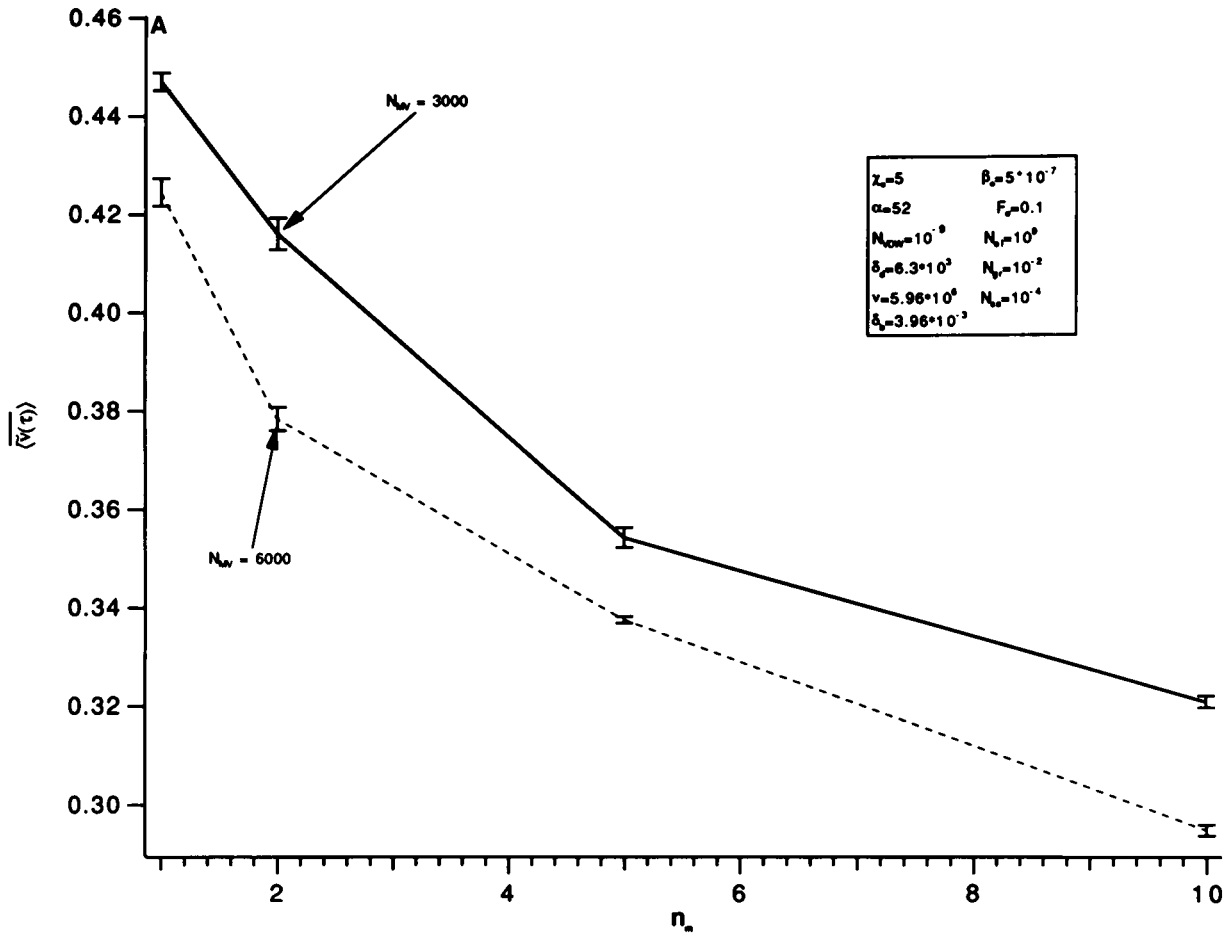

FIGURE 4 In these figures (*A–D*) we study the effect of the number of microvilli (N_{mv}) and the numbers of receptor per microvillus tip (n_m) on adhesion. (*A*) The population average rolling velocity $\overline{\langle \tilde{V}_y \rangle}$ is plotted as a function of n_m for two different values of N_{mv}. Expectedly, cells roll more slowly if there are more receptors or microvilli. (*B–D*) Three trajectories at different values of n_m = 5 of individual cells for same parameter values shown in Fig. 4 *A* that demonstrate the onset of a minimum in the variance at n_m = 5, N_{mv} = 6000. (*B*) The trajectory at n_m = 1, N_{mv} = 6,000 shows little binding occuring relatively infrequently, leading to sizeable changes in the velocity. (*C*) The trajectory at n_m = 5, N_{mv} = 6,000 shows substantial binding sufficient to cause cell rolling, but insufficient to slow the cell down below $\tilde{V}_y$ = 0.3, leading to a low variance. This rolling state is designated state II, according to the nomenclature introduced later in this paper. (*D*) The trajectory at n_m = 10, N_{mv} = 6,000 shows substantial binding which leads to occasional large excursions to slow rolling ($0.1 \leq \tilde{V}_y \leq 0.2$), therefore increasing the variance. Parameters are as shown or as in the caption for Fig. 3.

siveness. In addition, higher values of α, generated by lower shear rates, also lead to an increase of adhesion. The spring constant, σ, appears in both of these parameters, so it is reasonable to ask whether stiffer springs (higher values of σ and hence α), also lead to greater adhesion. In Fig. 6, we plot the population average velocity as a function of α. The curve labeled F_σ = 0.1 was generated by simultaneously varying the transition state spring constant σ_{ts} such that F_σ remained fixed. Although one would expect adhesion to be more likely as the spring gets stiffer and α increases, the cell rolls faster. There are two reasons behind this apparent inconsistency. First, because the forward reaction rate at any separation other than the equilibrium separation decreases considerably as σ_{ts} is increased, fewer bonds are able to form as σ is increased along this curve. Second, at fixed F_σ, the difference $\sigma - \sigma_{ts}$ increases as σ increases. At any separation, the rate of breakage increases considerably as $\sigma - \sigma_{ts}$ increases. Therefore, as α increases at constant F_σ, the rate of forward reaction is decreasing, and the rate of reverse reaction is increasing. The net effect is to have fewer tethers which outweighs their individual increase in strength.

We performed a second set of simulations to investigate which of these two effects, the decrease in forward reaction at higher σ_{ts}, or the increase in reverse reaction at higher $\sigma - \sigma_{ts}$, was the dominant determinant of the number of tethers. In this simulation, we allowed F_σ to vary, keeping $\sigma - \sigma_{ts}$ fixed, and hence, allowing σ_{ts} to increase as σ (and α) increases. In effect, this will decrease the forward reaction rate, but keep the reverse rate fixed. Here, as α increases, the rolling velocity drops sharply, suggesting the relationship between bond strain and the rate of bond breakage dominates over any effect on the rate of bond formation. Comparing to the case

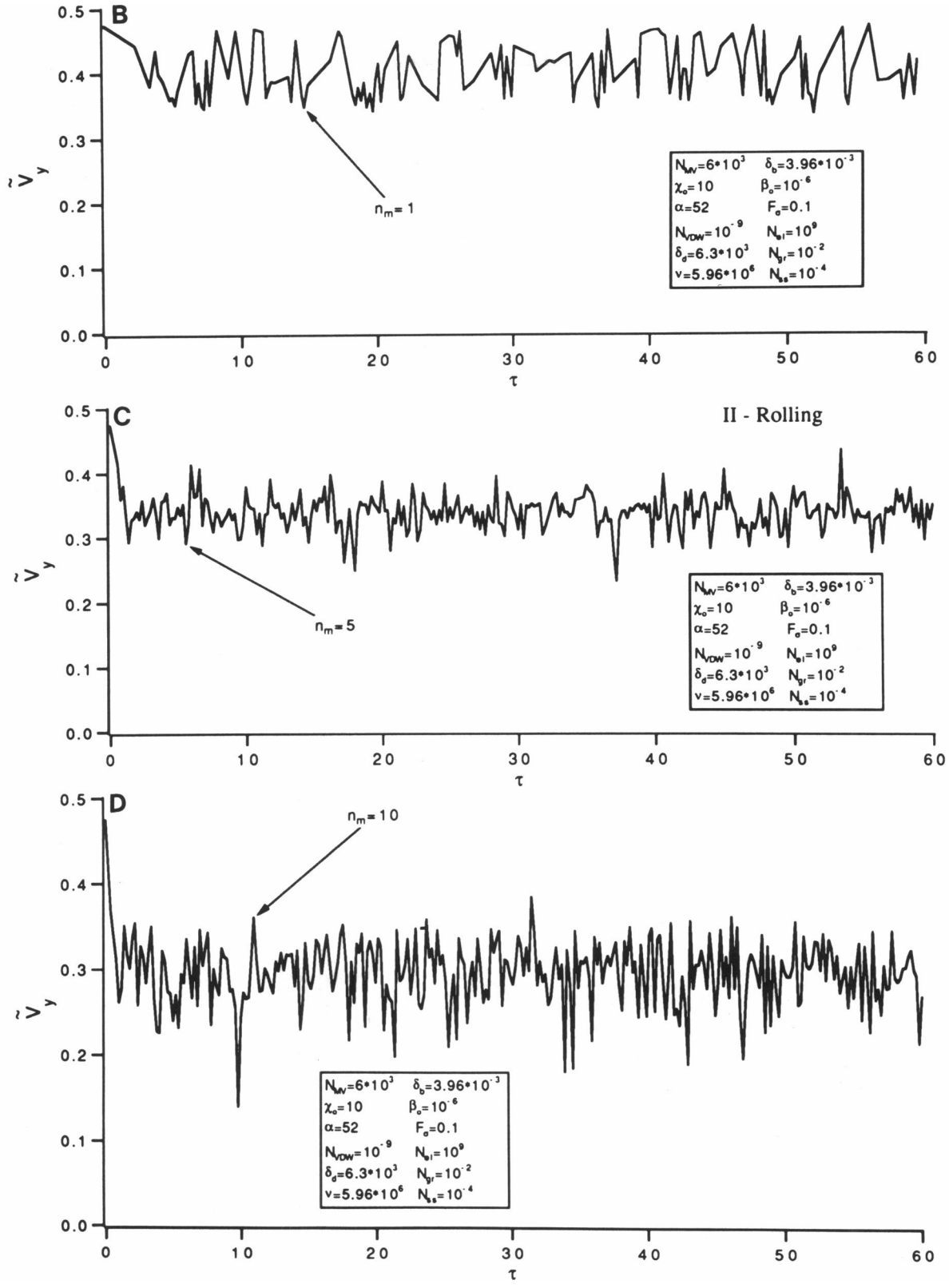

FIGURE 4 (continued)

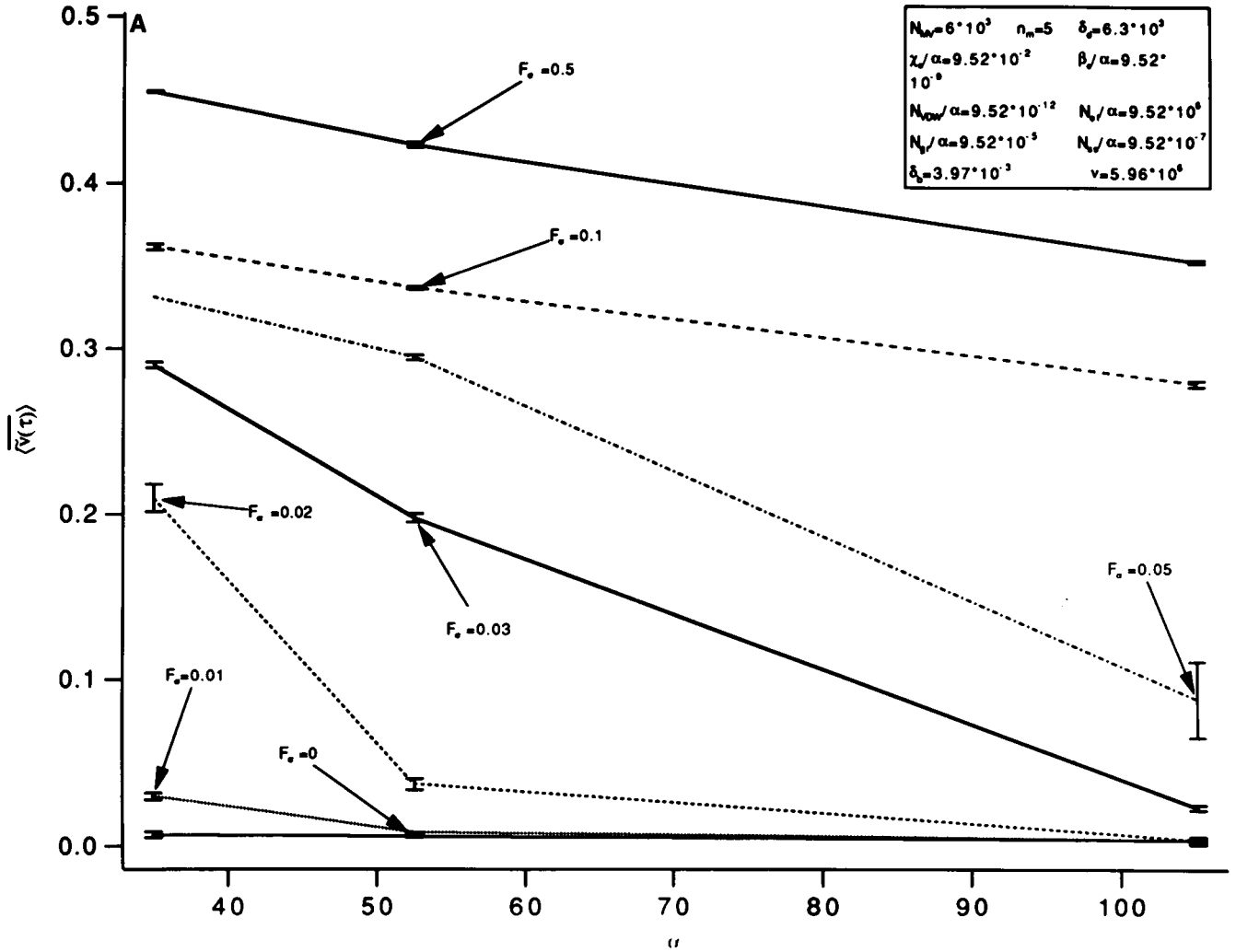

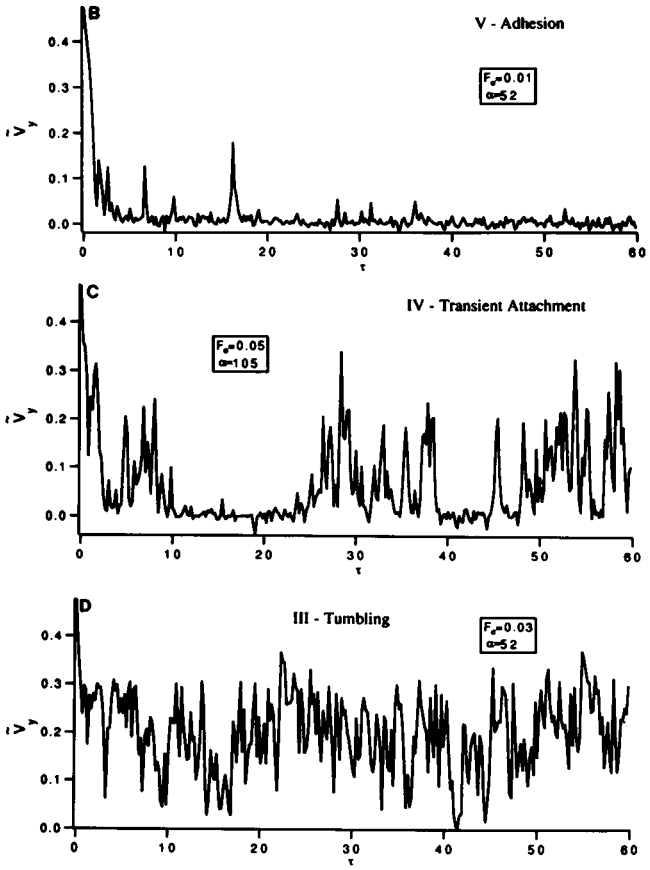

FIGURE 5 In Fig. 5 *A–D*, we explore the effect of F_σ, the fractional spring slippage, and α, the ratio of spring to fluid dynamic energy, on cell rolling and adhesion. (*A*) The population average rolling velocity $\langle \bar{V}_y \rangle$ is plotted as a function of F_σ and α. The expected trends are returned, where rolling is slower, or adhesion is more likely, if F_σ is smaller (the bonds break less quickly when they are extended) or if α is larger (the springs are stiffer, or the fluid energy is smaller). (*B–D*) Three example trajectories used to generate Fig. 5 *A* which indicate the wide range of observed motions which can be achieved with this method. (*B*) A trajectory where F_σ = 0.01 and α = 52, in which the cell appears largely adherent (state *V*). (*C*) A trajectory where F_σ = 0.05 and α = 105, in which the cell sometimes comes to a stop between periods of rolling (transient adhesion; state IV). (*D*) A trajectory where F_σ = 0.03 and α = 52, where the cell is moving during the entire simulation, but with a widely varying velocity (tumbling, state III). State II, rolling, was shown in Fig. 4 *C*.

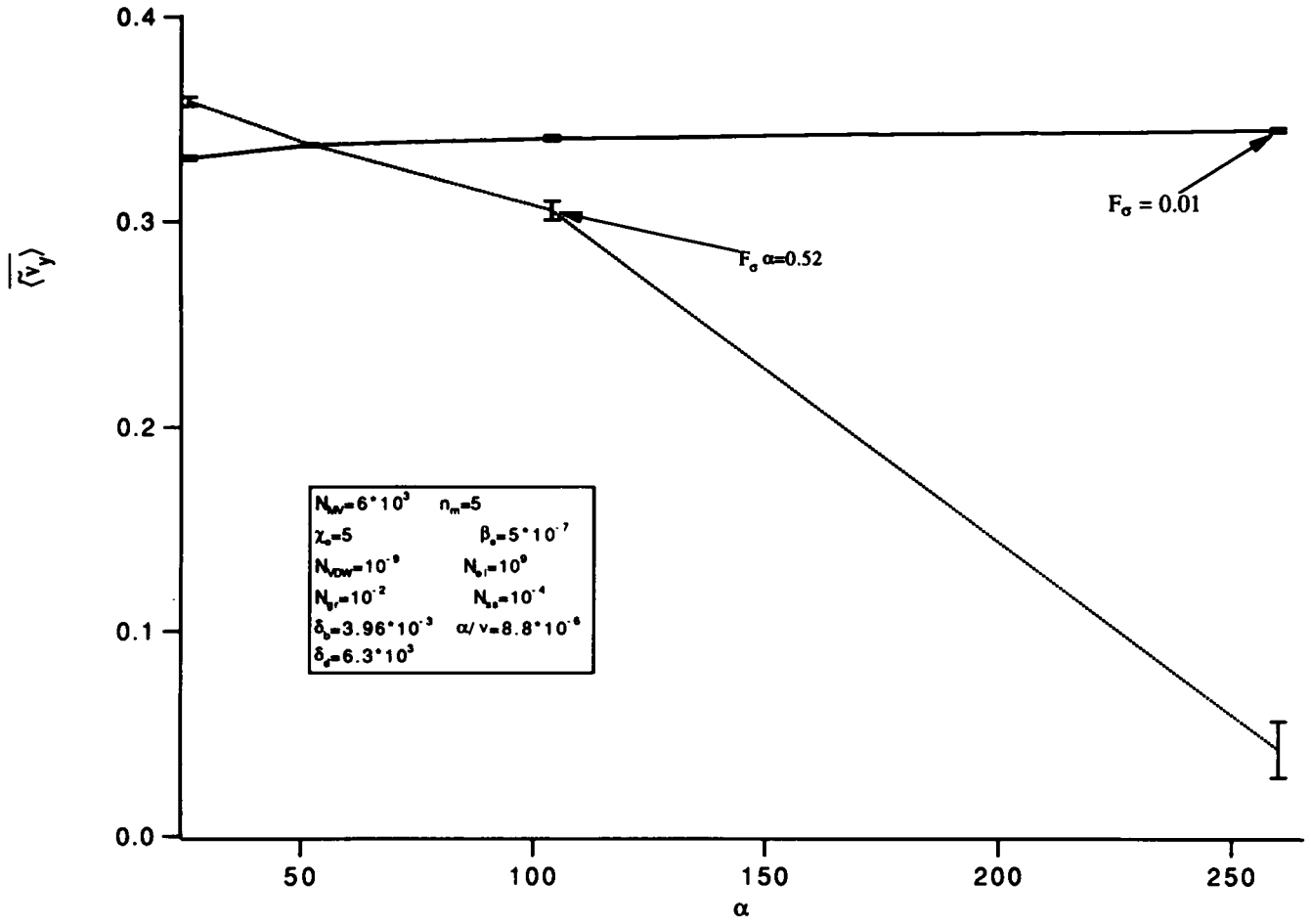

FIGURE 6 A plot of the population average translational velocity, $\langle \hat{V}_y \rangle$, as a function of the dimensionless ratio of spring to hydrodynamic energy, α, modulated in such a way to isolate the effect of spring stiffness on adhesion. The simulations are carried out in two ways; one in which the fractional spring slippage F_σ is held constant, and the other in which the magnitude of slippage is held constant ($F_\sigma\alpha = 0.52$). In the first case, the actual rate of rolling increases as the springs become stiffer. Despite their increased strength, the springs break more readily in response to extension, and the cell increases speed. When the spring constant is increased such that the rate of breakage remains constant, $F_\sigma\alpha = 0.52$, stiffer springs have the expected effect of further retarding cell motion.

where F_σ was fixed, at any value of α, the ability of bonds to withstand strain without significantly increasing the rate of breakage allows stiffer springs to exert a greater effect on cell motion, therefore slowing the cell down. To summarize this section, increases in bond strength will only significantly increase adhesion if the magnitude of slippage ($\sigma - \sigma_{ts}$) (and hence F_σ) remains small. This further emphasizes the fractional spring slippage is a key determinant of adhesion.

The binding between adhesion molecules is often characterized by an affinity, which in this paper is given in dimensionless form as κ. In Fig. 7, we show a plot of the mean rolling velocity as a function of affinity in the range from $10^5 \leq \kappa \leq 10^8$. Because κ is the ratio of forward (χ_o) and reverse reaction (β_o) rates, there are several different ways to examine binding at the different affinities. First, we determined the effect of changing the forward reaction rate, keeping the reverse reaction rate fixed, for diffusion limited binding (curve labeled $\beta_o = 5 \times 10^{-7}$; $\epsilon_d = 1$; Fig. 7). (The definition of ϵ_d is given in Appendix 2). This curve shows that as the affinity (χ_o) increases, binding increases, and the mean velocity decreases. Second, to test which is more important for adhesion at the same affinity, to have a faster forward reaction, or a slower reverse reaction, we generated a similar a curve by altering χ_o, keeping β_o fixed, but at 1% of the diffusion limit ($\beta_o = 5 \times 10^{-7}$; $\epsilon_d = 0.01$). At the same affinity, this curve differs from the previous curve in that both the forward and reverse reaction rates are two orders of magnitude lower. The plot shows clearly at 1% of the diffusion limit, the translational velocity is faster than when at the diffusion limit, suggesting it is more important to have a faster forward reaction for adhesion. This conclusion is substantiated by the third curve on this graph, labeled $\chi_o = 5$, $\epsilon_d = 1$, on which changes in affinity are achieved solely through changes in the reverse reaction rate. The result of changing the reverse reaction rate three orders of magnitude is no more than a

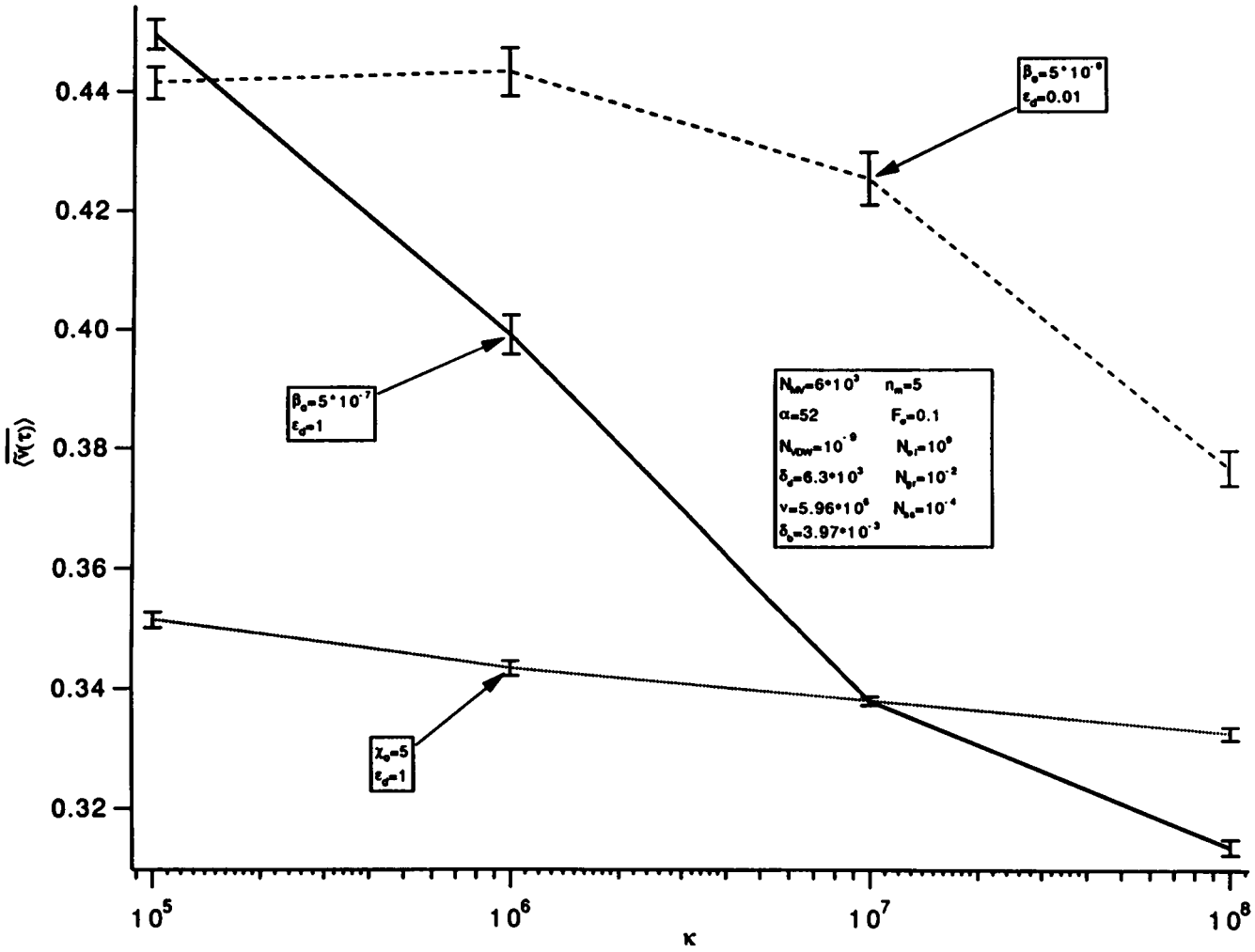

FIGURE 7 A plot of the population average translational velocity, $\langle \hat{V}_y \rangle$, as a function of the dimensionless affinity, κ, for three scenarios. In the first case, (*solid line*, $\beta_o = 5 \times 10^{-7}$, $\epsilon_d = 1$) we keep the reverse reaction rate constant while changing the forward reaction rate. These values are selected for diffusion-limited forward binding. In this case, changes in the affinity would result from a higher density of ligand, or a higher receptor diffusivity. As the affinity (or forward reaction rate) increases, a sizeable reduction in the rolling velocity results. In the second, (*dashed line*, $\beta_o = 5 \times 10^{-9}$, $\epsilon_d = 0.01$), the reverse reaction rate is again held constant, but the forward rate is assumed to be 1% of the diffusion limit. Hence, at the same affinity (κ), both the forward and reverse reaction rates are lower by a factor 100 compared to the $\beta_o = 5 \times 10^{-7}$ case. The rolling velocity also decreases with increasing affinity, but not as sharply as when at the diffusion limit, suggesting a higher forward reaction rate is more important than a lower reverse reaction rate for adhesion in this case. In the final case, (*dotted line*, $\chi_o = 5 \times 10^{-7}$, $\epsilon_d = 1$), the forward rate is held fixed, and the reverse rate is altered. Here, the rolling velocity is independent of affinity, because it only depends weakly on the reverse reaction rate. Two conclusions may be drawn in this case: the forward rate is the stronger modulator of adhesion, and the rolling velocity is not uniquely determined by the affinity itself.

5% change in the rolling velocity, again suggesting adhesion is very weakly dependent on the reverse reaction. Despite the inclination in the biological literature to assess the effectiveness of an adhesion molecule in terms of the affinity for ligand, the affinity itself is only weakly correlated to the dynamic process of adhesion in flow, in which the rates of reaction, specifically the forward rate of reaction for molecules of high affinity, plays a large role in determining the degree of binding.

We have demonstrated the ability of our method to recreate the wide variety of observations of adhesive behavior under flow by showing a variety of different representative trajectories in Fig. 4, *B–D* and Fig. 5, *B–D*. There are five basic observable types of behavior, each of which can be identified by a distinguishing Roman numeral: unbound (I); rolling at constant speed (II) (Fig. 4 *C*); tumbling, which suggests a largely rolling motion with very brief periods of adhesion (III) (Fig. 5 *D*); transient adhesion, which suggests significant periods of adhesion during which the cell remains motionless, followed by tumbling or rolling (IV) (Fig. 5 *C*); and adhesion, whose onset is sometimes instantaneous upon contact of the surface, where the cell is largely motionless for long periods of time (V) (Fig. 5 *B*).

Although such qualitative descriptions of adhesion are useful, it should be possible to devise statistical measures

which, in combination with the rolling velocity and the variance, can be used to characterize all of these motions. The mean velocity and the variance are useful in characterizing motions I, II, and III, but are ineffective in characterizing motion IV, and transitions from III to V (extremely brief to complete adhesion). Three simple measures that we propose are the frequency of adhesion, F_a, defined as the fraction of time possess a velocity $\tilde{V}_y < 0.001$, and the forward and reverse kinetic constants for attachment and detachment. The kinetic rate of attachment is defined as the inverse of the mean time before a moving cell becomes adherent; the kinetic rate of detachment is the inverse of the mean time before an adherent cell begins to move. This gives rise to rather simple mathematical definitions,

$$k_a = \frac{N_{\tilde{v}_y>0.001}}{\sum_{i=1}^{N_{\tilde{v}_y>0.001}} \Delta\tau_{i,N_{\tilde{v}_y>0.001}}} \tag{10}$$

$$k_d = \frac{N_{\tilde{v}_y<0.001}}{\sum_{i=1}^{N_{\tilde{v}_y<0.001}} \Delta\tau_{i,N_{\tilde{v}_y<0.001}}}. \tag{11}$$

In these expressions, $N_{\tilde{v}_y<(>)0.001}$ is the number of instances the cell is moving at the indicated velocity before the inequality is no longer satisfied, and $\Delta\tau_i$ is the time the cell was moving at the indicated velocity. The frequency of adhesion is essentially a measure of the ratio of the kinetic rate of attachment to the kinetic rate of detachment, or the equilibrium constant for attachment. If this ratio is high, the frequency of adhesion will approach 1; if it is low, the frequency will approach 0.

We plot in Fig. 8 the variation in F_a, k_a, and k_d as a function of α for different values of $F_\sigma \leq 0.05$, for which Fig. 5 has already provided information regarding the mean of the translational velocity in the y direction. In Fig. 8 *A*, we show F_A increases as α increases or as F_σ decreases. This is physically reasonable, because we would expect the cell to become less adherent (have a lower value for F_a) if the shear rate were higher, or if the bonds slip to a greater extent. Note in the lower left hand corner of Fig. 8 *A*, F_a is zero; the cells are not adherent, as the shear rate is too high and the slippage is too great to support binding. These trends are mirrored by the forward reaction rate for attachment, k_a, shown in Fig. 8 *B*. At any degree of slippage (constant F_σ), k_a increases as α increases. The rate of attachment is greater at lower shear rates, which is physically plausible. But the rate of attachment also increases as F_σ decreases. This might seem perplexing, because F_σ is an indicator of the degree of slippage and as such tells us how bonds break in response to strain, not how they form. In fact, for constant σ, lower values of F_σ mean higher values of σ_{ts}, which implies the rate of forward reaction should decrease at any separation. We believe this inconsistency is explained if one considers adhesion a process which requires the concerted effort of many adhesion molecules; a cell will not attach unless the adhesion molecules, especially those which form initial contacts, are particularly resistant to breakage. Therefore, the resistance of bonds to breakage is subtlely incorporated into the overall measurement of the attachment rate constant.

In Fig. 8 *C*, we examine the rate of detachment as a function of F_σ and α. Despite large values in the standard deviation for k_d, the mean of k_d shows the expected trends for $F_\sigma > 0$, where the rate of detachment is greater when the adhesion molecules slip (higher F_σ), or when α is lower (eg., higher shear rate). Several of these curves disappear when α is below a critical value, because in this region of parameter space, cells never attach, and it is thus impossible to determine the detachment rate constant. For $F_\sigma = 0$, the rate of detachment is independent of α, because the rate of bond breakage is unrelated to bond strain, and hence fluid forces acting to extend the bonds have no effect in increasing detachment. There are two contributing factors to the large standard deviation of detachment rate constants. First, in an ensemble of particles in a region of parameter space close to the adhesion limit, it is not unusual to find a only subset of the ensemble adhering. Those cells which do not adhere, while contributing information to the attachment rate constant ($k_a = 0$), do not contribute any information to the detachment rate constant. Whereas N cells may be involved in determining k_a, fewer than N are used to determine k_d, giving rise to a more error prone measurement. Second, an adherent cell with a tendency to detach may follow a wide variety of paths to motion. Such a cell may begin to move immediately upon the breakage of a single tether, or may crawl very slowly over the surface before moving at a perceptible speed. One can liken this to the wide variety of paths a ligand may take over a cell surface as it tries to escape cell surface receptors; the ligand can immediately dissociate, or diffuse along the surface, rebinding with other receptors many times before dissociation (Berg and Purcell, 1977; Northrup, 1988). Such a wide variety of dissociative trajectories naturally yields a wide spectrum dissociation times for the cell, and gives a large standard deviation.

Table 3 summarizes the measured values for $\langle\tilde{V}(y)\rangle$, $\langle(\tilde{V}(y) - \langle\tilde{V}(y)\rangle)^2\rangle$, F_a, and k_a, and k_d for each of the states I–V defined previously. For state I (unencumbered), the values of these measures are clear a priori. For state II, values are taken from Fig. 4 *C*, with $n_m = 5$, and $N_{mv} = 6{,}000$. For states III–V, values for the mean of the velocity are taken from Fig. 5 *A*, whereas values for the frequency of adhesion, and the attachment and detachment rate constants are taken from Fig. 8. (Figs. 5 and 8 are generated with the same parameters). For state V (adhesion), $F_\sigma = 0.01$ and $\alpha = 52$; for state IV (transient attachment), $F_\sigma = 0.05$ and $\alpha = 105$, and for state

III (tumbling), $F_\sigma = 0.03$ and $\alpha = 52$. The table shows the expected trends for each of these parameters; each state appears to be uniquely characterized by a different set of values for the statistical measures, and reinforces the utility of using these five parameters in quantitatively characterizing the full spectrum of possible cell motions on a surface.

COMPARISON TO EXPERIMENT

We use this simulation technique to understand the observation, recently made by many groups (Lawrence and Springer, 1991; Lawrence et al., 1990; Ley et al., 1991; von Adrian et al., 1991) that the initial rolling of neutrophils on the surface of endothelial cells in the microvasculature is mediated by binding between selectin molecules, notably LECAM-1 on the neutrophil surface, and its counter-selectin, CD62 (GMP-140), on the endothelial cell. Other adhesive molecular pairs, notably CD18 integrins on the neutrophil, and ICAM-1 on the endothelial cell, do not cause rolling, despite an equal affinity between CD62 and LECAM-1 as between CD18 and ICAM-1 (Lawrence and Springer, 1991; Lawrence et al., 1990). In specific, we wish to understand data recently published on cell rolling on lipid-linked CD62 and/or ICAM-1 monolayers in a parallel-plate flow chamber, taken by Lawrence and Springer (1991) in which a number of the parameters which are suspected of controlling adhesion, such as CD62 or ICAM-1 density, or flow rate, were systematically varied.

In matching these experiments, we concentrate on matching reported rolling velocity data of neutrophils on CD62 only, because the addition of ICAM-1 to CD62 monolayers only slightly augmented the degree of adhesion, and since adhesion on ICAM-1 layers alone at a shear stress of 1.8 dynes/cm^2 was negligible (Lawrence and Springer, 1991). Our first objective was to discover the appropriate region of parameter space to match this data. This endeavor was made possible by the separate measurement of many of the important parameters governing adhesion, as shown in Table 2. Several parameters are peculiar to the neutrophil system. First, the number of LECAM-1 receptors on the neutrophil was reported to be low, 2×10^4 (Lawrence and Springer, 1991), which gives an average number of receptors per microvilli tip $n_m = 0.465$. Second, we must consider the possibility that LECAM-1 molecules are concentrated on the tips of microvilli, since Picker and co-workers have presented electron micrographic evidence of this, using gold-labeled antibody against LECAM-1 (Picker et al., 1991). Because only two microvilli were shown in this paper, it is difficult to make conclusions about the quantitative level at which receptors are concentrated, or the uniformity of this effect across a single cell, or among cells in a population. Finally, the CD62/LECAM-1 bond is quite long, estimated to be ~50 nm, mostly caused by the extreme length for CD62 (Springer, 1990).

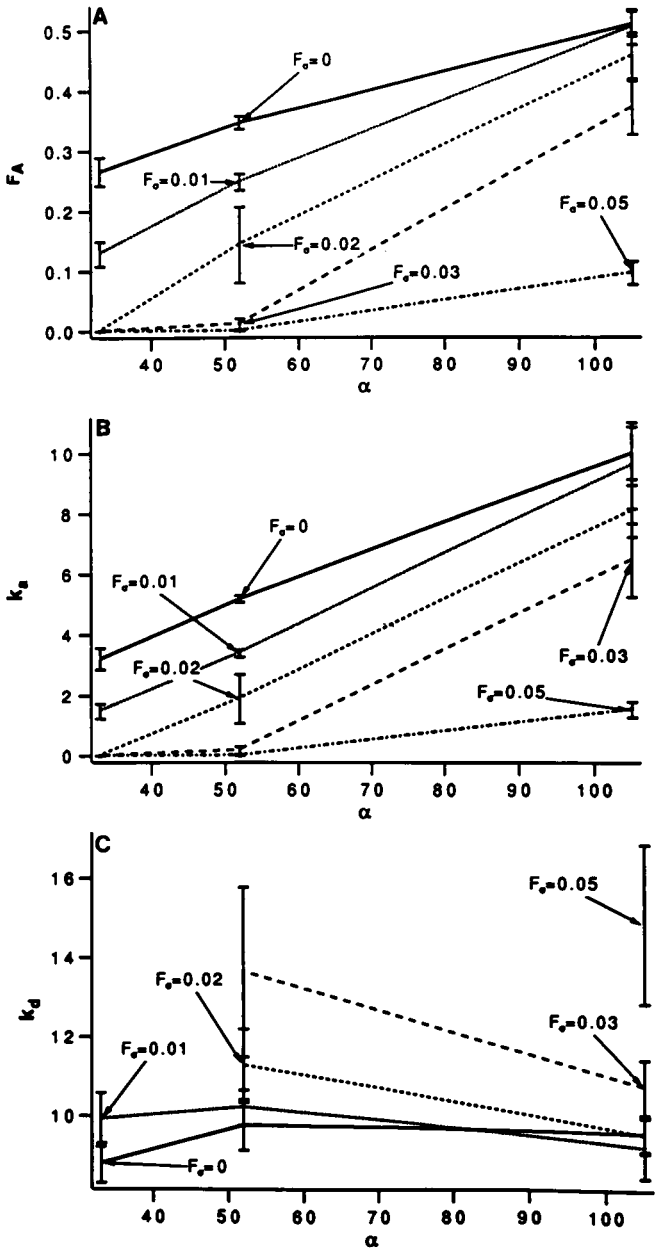

FIGURE 8 Three statistical measures are plotted as a function of α: F_A, the frequency of adhesion; k_a, the attachment rate constant; and k_d, the detachment rate constant. (*A*) The frequency of adhesion F_A increases as α increases, and as F_σ decreases, as expected. (*B*) The kinetic rate constant for adhesion increases as α increases, and as F_σ decreases, also as expected. (*C*) The kinetic rate for detachment, k_d, largely increases as α decreases, or as slippage (F_σ) increases. Three salient features of this graph are that some of the curves at higher values of F_σ appear incomplete, because k_d is indeterminant for nonadherent cells; that the standard deviations are rather large due to the large number of paths a cell may take before detachment; and that for low F_σ, k_d is independent of α, because bond breakage is largely independent of strain.

Using parameters from Table 2, and reported in the caption of Fig. 9, we attempted to match the

TABLE 3 **Example values for statistical measures of adhesion for five qualitatively different types of cell motion**

State	Description	$\overline{\langle \tilde{V}(y) \rangle}$	$\overline{\langle (\tilde{V}(y) - \langle \tilde{V}(y) \rangle)^2 \rangle}$	F_a	k_a	k_d
I	Unbound	0.48	0	0	0	ND*
II	Rolling	0.335	6.1×10^{-4}	0	0	ND*
III	Tumbling	0.19	6×10^{-3}	0.012	0.171	13.61
IV	Transient adhesion	0.09	7.2×10^{-3}	0.09	1.532	14.83
V	Adhesion	0.005	1.8×10^{-3}	0.249	3.392	10.21

* ND indicates the detachment rate constant could not be determined from this simulation, because the cell never attached.

value of $\overline{\langle \tilde{V}(y) \rangle} = 0.00844$ reported (Lawrence and Springer, 1991) at a shear stress of 180 dynes/cm^2 for a CD62 density of 200 molecules/cm^2. The parameters which we do not know a priori for this system are α, the ratio of the spring energy to the fluid energy, because of uncertainty in the spring constant; F_σ, the fractional spring slippage; and n_m, the number of receptors per microvillus tip, because we cannot discount evidence that the receptors are concentrated, but do not have any good quantitative value for the degree of concentration. Additionally, we do not know χ_o, the dimensionless forward reaction rate, principally because we do not know k_f^o. For these calculations, we assume the forward reaction is diffusion-limited (as fast as it can be), assuming the diffusion constant for the receptor is 10^{-9} cm^2/s (Axelrod et al., 1978; Jacobsen et al., 1984). The reverse rate is calculated using k_f^o the measured value for the affinity.

As one can imagine, many combinations of the constants α, F_σ, and n_m can give an appropriate fit to a single datum point. In Fig. 9, *A* and *B*, we show four such combinations. In Fig. 9 *A*, $\overline{\langle \tilde{V}(y) \rangle}$ was calculated with σ = 1 dyne/cm, whereas Fig. 9 *B* was calculated with σ = 2 dyne/cm; hence, the two figures are for different values of α. These values for the spring constant are selected based on theoretical estimates of the spring constant (Bell, 1978; Evans 1985*a,b;* Bell et al., 1984; Dembo et al., 1988), or measurements of the force to fracture glycophirin molecules from a red blood cell membrane (Evans et al., 1991). In each of these two figures, one finds two curves, each labeled with a different value of n_m. Those labeled $n_m = 0.465$ are calculated as if LECAM-1 receptors are randomly distributed over the cell surface; those labeled $n_m = 2.32$ are calculated as if LECAM-1 receptors are concentrated on microvilli tips by a factor of five over the randomly distributed case. In all cases, the calculations are carried out for different values of F_σ. We wish to determine the appropriate value for F_σ to describe the single datum point, labeled as a dotted line on these figures.

In Fig. 9 *A*, in which $\alpha = 69.4$, we see for $n_m = 0.465$, several values of $F_\sigma \leq 0$ match the data, all within 1% of the ideal bond limit ($F_\sigma = 0$). These are the only simulations in this paper extended into the catch bond limit, but catch bond behavior is not required to match the data, because $F_\sigma = 0$ appears acceptable. If n_m is increased to 2.32, the requirement on F_σ becomes less strict; a value of F_σ of 0.8% is needed to match the reported data. In Fig. 9 *B*, and $\alpha = 138.7$, where $n_m = 0.465$, a fractional spring slippage of 0.15% matches the data. Once again, as n_m is increased to 2.32, the tolerable fractional spring slippage is increased to 0.8%.

Comparisons between Fig. 9, *A* and *B*, lead to several conclusions. For all the parameter sets shown, a recreation of the cited rolling velocity data requires F_σ for the LECAM-1/CD62 bond to be less than 1%, exceedingly close to the ideal bond limit. We reach this conclusion despite our uncertainty about the degree to which LECAM-1 receptors are concentrated on microvilli tips (n_m), and the actual value of the spring constant (α). Of course, the concentration of receptors on the microvilli tips does relax the constraint on F_σ somewhat; for example, a percentage spring slippage of 0.8% can be tolerated if the receptors are concentrated, versus 0.15% if they are not (Fig. 9 *B*). Finally, the requirement on F_σ does not seem to be very sensitive to the spring constant (α). Comparing curves for $n_m = 0.232$ between Fig. 9, *A* and *B*, one sees the same percentage spring slippage, 0.8%, is required despite a factor of two difference in the spring constant.

In Fig. 10, we continue our analysis of rolling velocity data (Lawrence and Springer, 1991) for the effect of CD62 density on rolling velocity. Changes in ligand density are given by changes in χ_o. For the two sets of parameters (n_m, α, and F_σ) in Fig. 9 *B* which match the single reported datum point at 200 CD62 molecules/μm^2, we carry out calculations for both 50 and 400 CD62 molecules/μm^2, for which Lawrence and Springer (1991) also supplied data. In Fig. 10 *A*, we used the analysis from Fig. 9 *B*, in which $n_m = 0.465$, $\alpha = 138.7$, and $F_\sigma = 0.008$, and find extremely good agreement between data and the calculated simulations results. In Fig. 10 *B*, we also use analysis from Fig. 9 *B*, in which $n_m = 2.32$, $\alpha = 138.7$, and $F_\sigma = 0.0015$, and the agreement is much less impressive. Where $n_m = 2.32$, each microvillus tip is sufficiently adhesive to overcome deficiencies in the ligand density; hence, the simulated rolling velocity is weakly dependent on ligand density, much more weakly than in the experiments. These results imply that a random, rather than concentrated, distribution of receptors is better able to explain the reported rolling results. However,

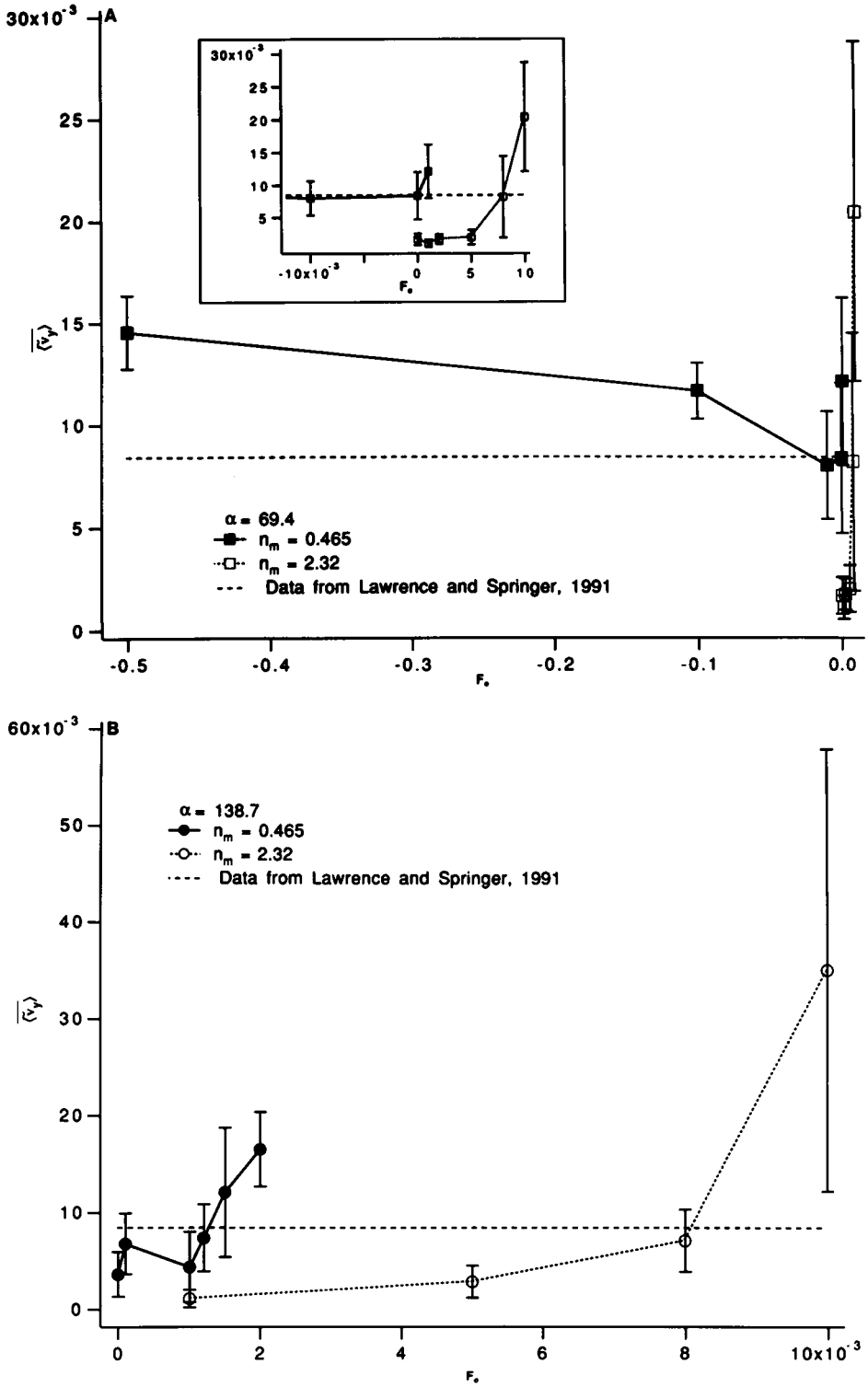

FIGURE 9 Examination of parameter space of α, n_m, and F_e, to determine the appropriate sets of these parameters which could match data for neutrophil rolling on CD62 selectin molecules at a shear stress of 1.8 dynes/cm^2 and CD62 density of 200 molecules/μm^2, given as a dashed line in these figures (Lawrence and Springer, 1991). In Fig. 9 *A*, $\langle \check{V}_y \rangle$ is plotted for $\alpha = 69.4$, as a function of F_e for two different values of n_m: 0.465 (■, *solid line*, corresponding to randomly distributed receptors), and 2.32 (□, *dotted line*, corresponding to concentrated receptors). In Fig. 9 *B*, $\langle \check{V}_y \rangle$ is plotted for $\alpha = 138.7$ as a function of F_e, also for $n_m = 0.465$ (●, *solid line*) and $n_m = 2.32$ (○, *dotted line*). The acceptable values for F_e come when the solid or dotted lines cross the dashed line representing the data. In all cases, F_e must be less than 0.01 to match the data. Other parameter values in these simulations are $\chi_o = 0.55$, $\beta_o = 2.7 \times 10^{-6}$, $\nu = 8.77 \times 10^6$, $\delta_b = 1.17 \times 10^{-2}$, $\delta_{mv} = 1.17 \times 10^{-1}$, $\delta_g = 4.7 \times 10^{-3}$, $N_{vdw} = 10^{-9}$, $N_{el} = 10^9$, $N_{ss} = 10^{-4}$, $N_{gr} = 10^{-4}$, $\delta_d^{-1} = 1.58 \times 10^{-4}$, and $\delta_1 = \delta_2 = 2.32 \times 10^{-3}$.

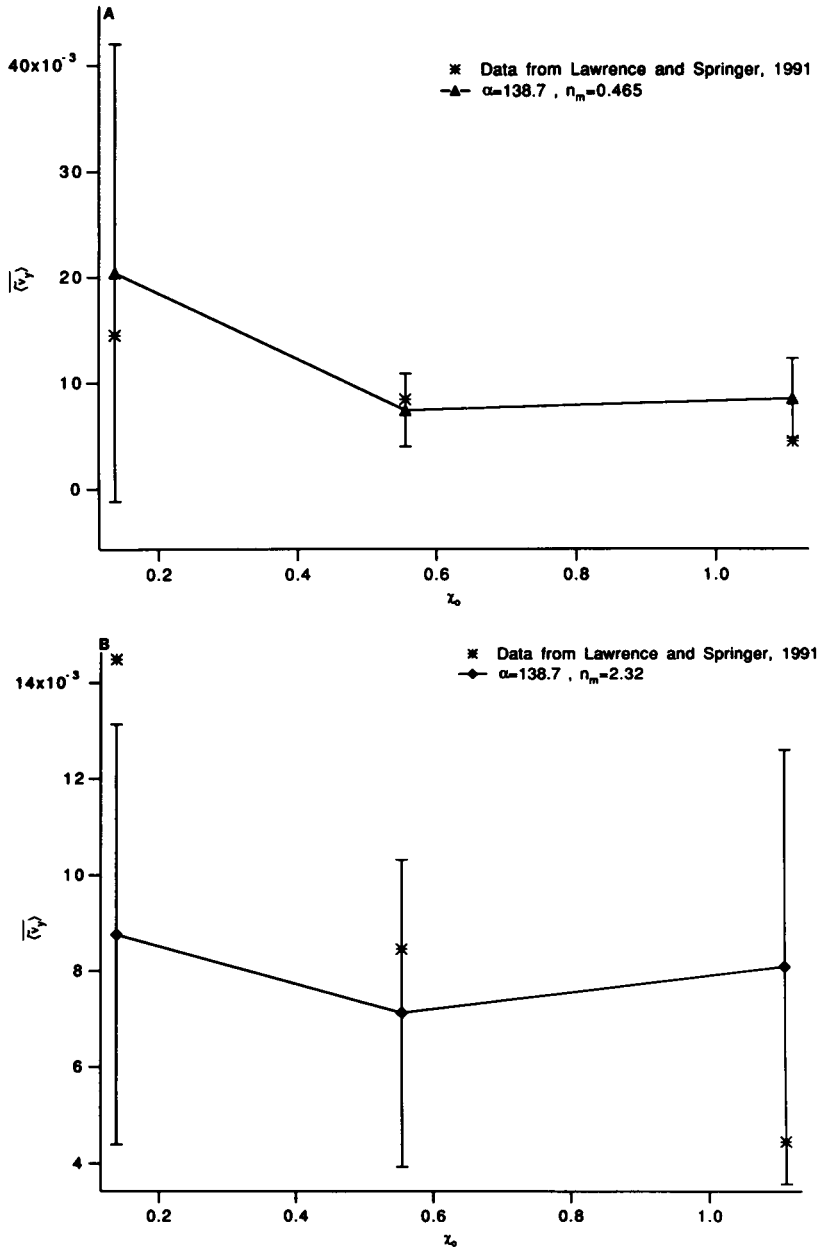

FIGURE 10 Fig. 10, *A* and *B* are two attempts at matching CD62 ligand density data given by Lawrence and Springer, 1991. As a starting point for these calculations, we took the two values of F_e which best fit the single datum point in Fig. 9 *B* (α = 138.7) for two different values of n_m (0.465 and 2.32), and then altered the dimensionless reaction rate χ_o to accommodate changes in the ligand density. In Fig. 10 *A*, calculated with n_m = 0.465 and F_e = 0.0012, the simulation results (▲) show good agreement with the data (*). In Fig. 10 *B*, calculated with n_m = 2.32 and F_e = 0.008, the simulation results (◆) show relatively poor agreement with the data (*), suggesting it is not necessary to invoke a concentration of LECAM-1 receptors at microvilli tips to explain the trend in rolling data with CD62 density. Other parameters are as in Fig. 9.

it would be naive to conclude as such. The best we can say is that at least in one case, the model can successfully predict the observed trend in rolling velocity with ligand density, and that not all parameter sets which match the single datum point at a density of 200 CD62 molecules/μm^2 match that trend.

DISCUSSION

We have presented a simulation method for the receptor-mediated binding of a microvilli-coated hard sphere to ligand-coated surfaces under viscous shear flow. The method allows us to quantify the role cell surface chemistry and microstructure play in cell adhesion. Parameters such as receptor-ligand binding constants, receptor-ligand bond strength and response to strain, receptor and ligand density, and the topology of the cell surface are all adjustable in our analysis. In addition, we can quantify the magnitude of the variability in adhesive phenotype that identically endowed cells can display. It would be of interest, and a subject of future work, to understand how

that variability compares to the variability one would expect from population heterogeneity.

This method is sufficiently robust to describe the entire spectrum of adhesive states from completely nonadhesive (unencumbered) to transient adhesion to irreversible attachment (Cozens-Roberts, 1990*c*; Doroszewski, 1980; Lawrence and Springer, 1991; Schmidt et al., 1990; Tissot et al., 1991; Tempelman and Hammer, 1990; Wattenbarger et al., 1990; House and Lipowsky, 1991). For example, while simulations of rolling match neutrophil adhesive phenomena (Lawrence and Springer, 1991), simulations of transient adhesion match phenomena observed for leukemia cells rolling on glass (Doroszewski, 1980), and simulations of firm, instantaneous attachment match experiments performed with glycophorin-reconstituted liposomes on lectin-coated surfaces (Wattenbarger et al., 1990). Although further simulations are necessary to make a rigorous comparison to adhesive phenomena involving smooth bodies (such as liposomes), the current model suggests all these manifestations of adhesion can be controlled at the molecular level without considering differences in surface morphology. To our knowledge, this is the first such model which can predict all these states. In addition, we point out several statistical measures which can be used to determine each of these states uniquely. Table 3 represents a clear demonstration that each of these states may be characterized by a unique set of these statistical parameters.

Figs. 6 and 7 address the role of spring stiffness and affinity, respectively, on adhesion. We show increasing spring stiffness leads to an increase in adhesiveness only if the breakage rate for extended tethers did not substantially increase. This seems to suggest bond breakage is more important than bond formation in maintaining adhesion. However, our study of the role of receptor-ligand affinity showed that changes in the forward binding rate had a greater effect on adhesion than changes in the reverse rate. The explanation of this apparent inconsistency is that both a high forward rate and a low breakage rate are simultaneously necessary to ensure adhesion will occur. In the spring stiffness calculations, the forward rate was sufficiently high, and the rate of breakage was limiting adhesion. In the affinity calculations, the rate of breakage was sufficiently low, and the rate of formation was limiting adhesion.

We have compared our analysis to experimental data published recently on neutrophil rolling on lipid-linked substrates of a CD62, an endothelial surface selectin, which showed that CD62 is unique in its ability to promote cell rolling, despite its presence is relatively low density (200 molecules/μm^2) (Lawrence and Springer, 1991). We predict the CD62/LECAM-1 bond is responsible for cell rolling because it is unique in its response to strain, with a fractional spring slippage, F_σ, below 0.01. We make this prediction despite some uncertainty about the degree of concentration of LECAM-1 on microvilli tips, and the strength of the CD62/LECAM-1 bond. Furthermore, this conclusion is not subject to change based on revelations regarding the forward reaction rate between CD62 and LECAM-1, because we have assumed the fastest possible reaction rate (diffusion limitation), and the true reaction rate must fall below this. If the reaction rate turns out to be slower, this will only place a more severe constraint on F_σ. This prediction is consistent with prediction made by Dembo and co-workers, which indicated F_σ must be less than 2% to match data on neutrophil rolling taken using intravital microscopy (Dembo et al., 1988; Atherton and Born, 1972, 1973).

Finally, by making comparisons between a single datum point and our simulations, we have been able to find several values of the spring constant (α), the number of receptors per microvillus (n_m) and the spring slippage F_σ which provide acceptable fits to neutrophil rolling data. We urge experimentalists interested in the neutrophil system to measure each of these parameters independently. Thus far, only one of these parameter sets can be used to successfully recreate observations of cell rolling on different densities of CD62 (Lawrence and Springer, 1991). It is encouraging that only some of the parameter sets fit the observed data, because it leaves open the possibility that further experiment and comparison to theory will allow indirect determination of the intrinsic molecular parameters for the CD62/LECAM-1 system from neutrophil adhesion experiments.

There are two limitations to the analysis in its current form. First, the simulations are lengthy, and it is not possible to obtain information about the adhesive behavior of an ensemble of cells rapidly. For example, we estimate the simulations presented in this paper alone represent 6,000 h of computer time using a Digital Decstation 5000 workstation. It would be of interest to develop, in parallel, an analytical method based on stochastic differential equation theory (Gardiner, 1985). However, our observations of the degree of fluctuation in binding even for cells rolling at apparently constant rates suggest some statistical method (either simulation or stochastic theory) is necessary to describe this type of dynamic adhesion. For example, for no cell simulated in this paper was the number of receptors bound at any one time greater than 100, and typical variances indicate fluctuations are 20% of this number or greater. This, coupled with the argument that the first site of binding is the microvillus, and that for typical receptor densities the mean number of receptors per microvillus tip is quite low, indicates the number of receptors involved is too small to validate a deterministic model. This argument has also been forcefully made by Cozens-Roberts and co-workers (Cozens-Roberts et al., 1990*b*, *c*) to explain observations on the detachment of antibody-coated hard spheres from surfaces.

The second limitation is the absence of deformation,

either on a microstructural or cellular level. Microstructural deformation can be quite easily incorporated into this model, by modeling microvilli as viscoelastic elements with their own viscosity and elasticity constants (DiMilla et al., 1991). These constants have not been determined for microvilli, to our knowledge, but reasonable guesses could be applied to determine the effect of microstructural deformation on adhesion. These calculations are also planned. The problem of macroscopic deformation is more difficult to address, but it may be possible to impose integral relations for the energetics of deformation upon the current formalism to calculate the true force and torque exterted by external flow on a deformed structure (Evans and Yeung, 1989; Schmid-Schönbein et al., 1987; Lipowsky et al., 1991). Such an extension to this work would be particularly helpful in tumor cell adhesion, because it is suspected that metastasizing tumor cells have grossly different abilities to deform than their nonmetastasizing counterparts (Weiss, 1990).

Finally, this manuscript suggests that two types of experimental studies are needed to fully characterize adhesion under dynamic fluid flow conditions. First, model studies, using cells or hard spheres binding to substrates of well-defined chemistry in hydrodynamic flows, and the report of cell velocities in such experiments, would be of critical importance in verifing the model, as well as our understanding of the factors which control adhesion. Second, the measurement of molecular binding constants is of critical importance. Because adhesion in flow is dynamic, it is important to determine kinetic rate constants for binding of adhesion molecules. It is also wise to understand quantitatively how adhesion molecules respond to strain, using techniques such as the surface forces apparatus (Israelachvili, 1985; Helm et al., 1991). Our simulations tell us the molecular parameters which are most important in modulating adhesion under flow are, aside from receptor number and ligand density, k_f^o, k_r^o, σ, and σ_{ts}. These parameters are difficult to determine and are not known for any molecular system involved in adhesion, but that will have to change before our knowledge of cell rolling and adhesion can be complete.

APPENDIX 1

To simulate the binding and breakage of adhesive tethers, consider a single time step in the simulation, Δt. For a free receptor located on a microvillus, a distance x_m from the substrate, and assuming x_m does not change substantially during this time step (an Eulerian approximation), the probability that a receptor will become bound during this time step, P_b, is governed by the differential equation,

$$\frac{dP_b}{dt} = k_f(1 - P_b), \tag{A1}$$

where $1 - P_b$ is the probability that the molecule is free during the time interval. Integrating from 0 to Δt, the probability of binding at the end of the time step is

$$P_b = 1 - \exp(-k_f \Delta t). \tag{A2}$$

During each time step of the simulation the probability of binding is calculated for each receptor on all microvilli tips, and binding is determined by comparing a random number generated for each receptor to this probability; if the random number is less than P_b, a bond is established at the end of the time interval (because we cannot say when in the interval the bond appeared).

Similarly, the probability that a bond which already existed prior to the current time step will break during Δt is

$$P_r = 1 - \exp(-k_r \Delta t), \tag{A3}$$

and if the generated random number is less than this probability, the bond breaks during this interval. In Eq. A3, k_r is based on the length of the bond.

As shown in Fig. 2, we use two coordinate systems to fully characterize our problem. A cartesian coordinate system is centered on the cell. In addition, each microvillus is assigned a unique position on the cell surface in spherical coordinates. (In this problem, $0 \le \varphi \le \pi$, $0 \le \theta \le 2\pi$, and points on the cell surface can be given in either coordinate system with the following relationships: $y = R_{ch} \sin \varphi \sin \theta$, $z = R_{ch} \cos \varphi$, $x = h + R_{ch}(1 - \sin \varphi \cos \theta)$, where h is the minimum separation distance between the cell and the surface.) We determine the instantaneous translational and angular velocities of the cell in all cartesian directions. Any cell motion will give rise to motions of its associated rigid structures; therefore, one must keep track of the positions of the microvilli as the cell moves with time. This requires a straightforward translation between cartesian and spherical coordinates to update the positions of the microvilli.

We assume the molecules emanate from the center of the microvillus, and do not move laterally across the microvillus tip as a forces are applied to it; therefore, tracking the position of the microvillus tip $\vec{x}_m = (x_m, y_m, z_m)$ is tantamount to tracking the point at which the adhesion molecule is tethered to the cell. On the surface, the coordinates of the surface attachment point are $\vec{x}_o = (x_o, y_o, z_o)$. We assume the molecule is rigidly attached to the surface; however, because the coordinate system is in the cell's reference frame, translational motion of the cell will result in a net change in (x_o, y_o, z_o) with time. Each bond is described by a time-varying vector $\vec{x}_b = \vec{x}_o - \vec{x}_m$, from which one can calculate the force and torque in each cartesian direction from Eq. 5 as

$$F_x = \sigma(|\vec{x}_b| - \lambda)\left(\frac{x_o - x_m}{|\vec{x}_b|}\right)$$

$$F_y = \sigma(|\vec{x}_b| - \lambda)\left(\frac{y_o - y_m}{|\vec{x}_b|}\right)$$

$$F_z = \sigma(|\vec{x}_b| - \lambda)\left(\frac{z_o - z_m}{|\vec{x}_b|}\right); \tag{A4}$$

$$C_x = R_{ch}[F_x \sin \varphi_m \sin \theta_m - F_y \cos \varphi_m]$$

$$C_y = R_{ch}[F_x \cos \varphi_m - F_z \sin \varphi_m \cos \theta_m]$$

$$C_z = R_{ch}[F_y \sin \varphi_m \cos \theta_m - F_x \sin \varphi_m \sin \theta_m]. \tag{A5}$$

The net adhesive force and torque in each direction are calculated by summing these expressions over all tethers at every time point, and in combination with colloidal forces (calculated in Appendix 2) are used to derive the vector of forces (Eq. 8) and hence, the vector of velocities using Eq. 6 in the text. After the velocities are known, the positions of endpoints of each adhesive tether are updated during each time step. Because the cartesian coordinate system is in the cell's reference frame, the positions of the microvilli are determined by rectifying the cartesian angular velocities (Ω_i) into changes in θ and φ with time, and updating the θ and φ positions of each microvillus and bond. The positions of the end of the adhesion molecule on the substrate is updated using the translational velocities of the cell relative to the fixed surface. The equations necessary to update either the positions of the microvilli tips (or

end of tethers attached to the cell) or the end of molecules attached to the substrate, are

$$\frac{di_o}{dt} = -V_i,\ i = x, y, z \tag{A6}$$

$$\frac{d\varphi_m}{dt} = -\sin\theta_m\Omega_x + \cos\theta_m\Omega_y \tag{A7}$$

$$\frac{d\theta_m}{dt} = -\frac{\cos\varphi_m\cos\theta_m}{\sin\varphi_m}\Omega_m - \frac{\cos\varphi_m\sin\theta_m}{\sin\varphi_m}\Omega_y + \Omega_z. \tag{A8}$$

The logic of the simulation is as follows. First, the microvilli are placed on the surface, by a hard disk overlap algorithm, in which a position for each new microvillus is generated by random sampling and if a new disk overlaps any preexisting microvillus, it is rejected. Then, receptors are placed on the microvilli tips by sampling the cumulative probability distribution corresponding to the Poisson distribution (Eq. 4). (Because both of these steps require random number sampling, they introduce a level of statistical variability). Then, the simulation is started at $t = 0$ for time steps Δt. At each time t, random number generation, in conjunction with the calculated probability for bond formation P_f, is used to determine whether any bonds will form by $t + \Delta t$. These bonds are placed in their appropriate position at $t + \Delta t$, because we can not say when during Δt they appeared. Second, any bonds which already existed at time t are sampled to determine if they will be broken by $t + \Delta t$, and it is assumed that if they are, they disappear at $t + \Delta t$. Based on the known velocities of the cell at time t, the positions of all microvilli are updated during the simulation, giving new positions at $t + \Delta t$. At $t + \Delta t$, the forces imparted by the bonds which now exist, along with the colloidal and hydrodynamic forces, are used to calculate the velocity of motion at the time $t + \Delta t$. This loop is completed for each time step, until $t = t_{end}$ is reached. At simulation's end, a variety of statistical measures, discussed in the results section, are used to analyze the translational and angular velocities of motion.

APPENDIX 2

In this Appendix, we indicate how colloidal forces and rates of reaction are determined in our analysis. For calculating colloidal interactions, we use the fact that the tip of the microvillus dominates over all other surfaces (the remainder of the microvillus, or the cell body itself) in influencing the colloidal interactions, because most colloidal interactions have a very strong decay with distance, and the length scale for this decay is usually smaller than the length of an individual microvillus (Bongrand and Bell, 1984; Israelachvili, 1985). Therefore, it is necessary to calculate all colloidal forces for each microvillus, and sum over all microvilli to determine the net colloidal body force.

The van der Waals attraction is given (Hiemenz, 1986):

$$F_{vdw} = \frac{A_H A_{mv}}{6\pi}\sum_{\text{microvilli}} x_m^{-3}. \tag{A9}$$

Here, A_H is the Hamaker constant. The gravitational body force is given

$$F_{gr} = {}^4/_3\pi(\rho_c - \rho_m)R_{ch}^3 g, \tag{A10}$$

where ρ_c is the cell density, ρ_m is the medium density, and g is the gravitational constant.

It is known that two major forces exist in biological systems at distances from 50 to 250 Å: the electrostatic force, which is often repulsive (when the charges are of the same sign), and the steric stabilization force, which occurs due to the overlap of molecular chains (Bongrand and Bell, 1984). For the electrostatic interactions, we use the expression derived by Ohshima and co-workers in the limit of small Debye-Hückel length (Ohshima et al., 1987),

$$F_{el} = \frac{e^2 z_1 z_2 N_1 N_2 A_{mv}}{2\epsilon_r\epsilon_o\delta^2}\sinh\delta L_1 \sinh\delta L_2 \sum_{\text{microvilli}} e^{-\delta x_m}. \tag{A11}$$

Here, e is the fundamental electric charge, L_1 and L_2 are the thicknesses of the molecular layers associated with the cell and ligand layers, z_i and N_i are the valencies and charge densities in each layer, ϵ_o is the electrical permittivity, and ϵ_r is the relative permittivity, and δ is the inverse Debye-Hückel length. Finally, the steric stabilization force was estimated by Bongrand and Bell from the work on steric stabilization of Napper (Bongrand and Bell, 1984; Napper, 1983):

$$F_{ss} = \lambda_{ss}A_{mv}\sum_{\text{microvilli}} x_m^{-2} \quad x_m \le L_g$$
$$= 0 \qquad\qquad\qquad x_m \ge L_g, \tag{A12}$$

in which λ_{ss} is a constant determining the strength of the interaction due to chemistry of the two overlapping layers, and L_g is thickness of the glycocalyx at overlap of layers L_1 and L_2, where $L_g = L_1 + L_2$. The net colloidal force acting on the body is the sum of Eqs. A9–A12,

$$F_x^c = F_{vdw} + F_{gr} + F_{el} + F_{ss}, \tag{A13}$$

where the subscript "x" denotes directionality.

We also wish to define the concept of diffusion-limitation in reaction, introduced in the discussion of Fig. 7. We have modeled the substrate as a uniformly reactive surface; therefore the forward reaction rate k_f^o is the product of $k_f N_l$, where N_l is the density of ligand on the substrate. It is well known that k_f^o, the overall reaction rate, is properly expressed (Bell, 1978),

$$k_f^o = \frac{k_{+1}k_+}{k_{+1} + k_-}, \tag{A14}$$

where k_+ and k_- are forward and reverse rates for encounter between complimentary molecules, and k_{+1} and k_{-1} are forward and reverse intrinsic rates of reaction. When $k_- \gg k_{+1}$, we are in the diffusion limit, where

$$k_f^o = k_+ = 2\pi D \tag{A15}$$

where D is the surface diffusivity of the receptor molecule. One can generalize this expression to regimes outside of the diffusion limit,

$$k_f^o = k_+\epsilon_d, \tag{A16}$$

where ϵ_d is the fraction of the diffusion limit (Bell, 1981). As ϵ_d becomes smaller than one, we approach the reaction limit. For the reverse reaction,

$$k_r^o = k_-\frac{k_{-1}}{k_{+1}}\epsilon_d. \tag{A17}$$

In any case, the equilibrium constant can be written

$$K = \frac{k_+k_{+1}}{k_-k_{-1}}, \tag{A18}$$

which is independent of transport considerations.

APPENDIX 3

This section defines the dimensionless scaling and resulting parameters of the governing equations in this system. Because the motion of cells is driven by the external hydrodynamic flow, the appropriate time scale is $\dot\gamma^{-1}$, where $\dot\gamma$ is the shear rate. Defining the following dimensionless translational and angular velocities, and scaling all forces to $6\pi\mu\dot\gamma R_{ch}^2$

and all torques to $6\pi\mu\dot{\gamma}R_{ch}^3$, one obtains a set of dimensionless equations and associated dimensionless groups, equivalent in information content to Eqs. 1–3, 5–8, and A1–A18. The appropriate scales and dimensionless groups are

$$\tau = t\dot{\gamma} \quad \tilde{V}_i = \frac{V_i}{\dot{\gamma}R_{ch}} \quad \tilde{\Omega}_i = \frac{\Omega_i}{\dot{\gamma}}$$

$$\alpha = \frac{\sigma}{6\pi\mu\dot{\gamma}R_{ch}} \quad \nu = \frac{\sigma R_{ch}^2}{k_bT} \quad \nu_{ts} = \frac{\sigma_{ts}R_{ch}^2}{k_bT} \quad F_\sigma = \frac{\sigma - \sigma_{ts}}{\sigma}$$

$$\kappa = \frac{k_f^o N_l}{k_r} \quad \chi_o = \frac{k_f^o}{\dot{\gamma}} \quad \beta_o = \frac{k_r^o}{\dot{\gamma}} \quad n_m = \frac{R_T A_{mv}}{A_c}$$

$$N_{vdw} = \frac{A_H A_{mv}}{36\pi^2\mu R_{ch}^5\dot{\gamma}}$$

$$N_{el} = \frac{e^2 z_1 z_2 N_1 N_2 A_{mv}\delta_d^{-2}\sinh(\delta_1\delta_d)\sinh(\delta_2\delta_d)}{12\,\epsilon_o\epsilon_r\pi\mu\dot{\gamma}}$$

$$N_{gr} = \frac{2\Delta\rho R_{ch}g}{9\mu\dot{\gamma}} \quad N_{ss} = \frac{\lambda_{ss}A_{mv}}{6\pi\mu\dot{\gamma}R_{ch}^4}$$

$$\delta_b = \frac{L_b}{R_{ch}} \quad \delta_d^{-1} = \frac{L_{dh}}{R_{ch}} = \frac{1}{\delta R_{ch}} \quad \delta_g = \frac{L_g}{R_{ch}}$$

$$\delta_{mv} = \frac{L_{mv}}{R_{ch}} \quad \delta_{1,2} = \frac{L_{1,2}}{R_{ch}}. \tag{A19}$$

We have made an attempt to estimate values of all parameters from previous sources. These estimates, for both precursor dimensional and dimensionless parameters, are shown in Tables 1 and 2. Note in Table 2 we have drawn a distinction between general parameters which might be suitable for all leukocytes, and neutrophils. Using the above dimensionless variables, the governing equations for the systems become: (*a*) kinetics of binding and breakage during a time step $\Delta\tau$:

$$\chi = \chi_o \exp\left(-\frac{\nu_{ts}}{2}(\tilde{x}_m - \delta_b)^2\right) \tag{A20}$$

$$\beta = \beta_o \exp\left(\frac{(\nu - \nu_{ts})}{2}(\tilde{x}_m - \delta_b)^2\right) \tag{A21}$$

$$P_b = 1 - e^{-\chi\Delta\tau} \tag{A22}$$

$$P_r = 1 - e^{-\beta\Delta\tau}; \tag{A23}$$

(*b*) dimensionless forces and torques imparted by bonds (all forces are scaled to $6\pi\mu\dot{\gamma}R_{ch}^2$; all couples scaled to $6\pi\mu\dot{\gamma}R_{ch}^3$):

$$\tilde{F}_i = \alpha(|\tilde{\mathbf{x}}_b| - \delta_b)\left(\frac{i_o - i_m}{|\tilde{\mathbf{x}}_b|}\right); \quad i = x, y, z \tag{A24}$$

$$\tilde{C}_x = (\tilde{F}_x \sin\varphi_m \sin\theta_m - \tilde{F}_y \cos\varphi_m) \tag{A25}$$

$$\tilde{C}_y = (\tilde{F}_x \cos\varphi_m - \tilde{F}_z \sin\varphi_m \cos\theta_m) \tag{A26}$$

$$\tilde{C}_z = (\tilde{F}_y \sin\varphi_m \cos\theta_m - \tilde{F}_x \sin\varphi_m \sin\theta_m) \tag{A27}$$

$$|\tilde{\mathbf{x}}_b| = \frac{((x_o - x_m)^2 + (y_o - y_m)^2 + (z_o - z_m)^2)^{1/2}}{R_{ch}}; \tag{A28}$$

(*c*) dimensionless colloidal force:

$$\tilde{F}_x^c = N_{vdw}\sum_m \tilde{x}_m^{-3} + N_{gr} + N_{el}\sum_m e^{-\delta_d\tilde{x}_m} + N_{ss}\sum_m \frac{1}{\tilde{x}_m^2}H(\delta_g - \tilde{x}_m) \tag{A29}$$

(in this expression, summation is over the microvilli, designated "*m*"); (*d*) dimensionless force and torque balances:

$$\text{force in } x: \quad F_7(\check{h})\tilde{V}_x = \sum_b \tilde{F}_x + \tilde{F}_x^c; \tag{A30}$$

$$\text{force in } y: \quad F_3(\check{h})\tilde{V}_y + F_2(\check{h})\tilde{\Omega}_z = \sum_b \tilde{F}_y + F_5(\check{h}); \tag{A31}$$

$$\text{force in } z: \quad F_3(\check{h})\tilde{V}_z + F_2(\check{h})\tilde{\Omega}_y = \sum_b \tilde{F}_z; \tag{A32}$$

$$\text{torque in } x: \quad F_8(\check{h})\tilde{\Omega}_x = \sum_b \tilde{C}_x; \tag{A33}$$

$$\text{torque in } y: \quad F_4(\check{h})\tilde{V}_z + F_1(\check{h})\tilde{\Omega}_y = \sum_b {}^3\!/_4\,\tilde{C}_y; \tag{A34}$$

$$\text{torque in } z: \quad F_4(\check{h})\tilde{V}_y + F_1(\check{h})\tilde{\Omega}_z = \sum_b {}^3\!/_4\,\tilde{C}_z + \frac{F_6(\check{h})}{2}. \tag{A35}$$

In these expressions, summation is over the bonds, designated "*b*." $F_i(\check{h})$ are hydrodynamic functions. F_1 through F_6 are given by Goldman, Cox, and Brenner (Goldman et al., 1967*a*,*b*). F_7 is given by Brenner (1961), and F_8 is given by Jeffrey (1915);
and (*e*) translation and rotation of molecules:

$$\frac{d\tilde{i}_o}{d\tau} = -\tilde{V}_i; \quad i = x, y, z \tag{A36}$$

$$\frac{d\varphi_m}{d\tau} = -\sin\theta_m\tilde{\Omega}_x + \cos\theta_m\tilde{\Omega}_y \tag{A37}$$

$$\frac{d\theta_m}{d\tau} = -\frac{\cos\theta_m\cos\varphi_m}{\sin\varphi_m}\tilde{\Omega}_x - \frac{\sin\theta_m\cos\varphi_m}{\sin\varphi_m}\tilde{\Omega}_y + \tilde{\Omega}_z. \tag{A38}$$

These equations are solved according to the methodology described in Appendix 1, although in dimensionless form. The objective is to solve for the dimensionless translational and angular velocities as a function of dimensionless time τ.

The author acknowledges useful discussions with Micah Dembo and Thanasis Panagiotopoulos during the course of this work. This work was supported by National Science Foundation Research Initiation Award, EET-8808079, and by Cornell University's Moore Undergraduate Research Program.

Received for publication 1 November 1991 and in final form 17 February 1992.

REFERENCES

Atherton, A., and G. V. R. Born. 1972. Quantitative investigations of the adhesiveness of circulating polymorphonuclear leukocytes to blood vessel walls. *J. Physiol. (Lond.)*. 222:447–474.

Atherton, A., and G. V. R. Born. 1973. Relationship between the velocity of rolling granulocytes and that of blood flow in venules. *J. Physiol. (Lond.)*. 233:157–165.

Axelrod, D., A. Wright, W. Webb, and A. Horowitz. 1978. Influence of membrane lipids on acetylcholine receptor and lipid probe diffusion in cultured myotube membrane. *Biochemistry*. 17:3604–3609.

Bell, G. I. 1978. Models for the specific adhesion of cells to cells. *Science (Wash. DC)*. 200:618–627.

Bell, G. I. 1981. Estimate of the sticking probability for cells in uniform shear flow with adhesion caused by specific bonds. *Cell Biophys.* 3:289–304.

Bell, G. I., M. Dembo, and P. Bongrand. 1984. Cell adhesion: competition between nonspecific repulsion and specific bonding. *Biophys. J.* 45:1051–1064.

Berg, H. C., and E. M. Purcell. 1977. The physics of chemoreception. *Biophys. J.* 20:193–219.

Bongrand, P., and G. I. Bell. 1984. Cell–cell adhesion: parameters and possible mechanisms. *In* Cell Surface Dynamics: Concepts and Models. A. S. Perelson, C. DeLisi, and F. Wiegel, editors. Marcel Dekker, Inc., New York. 459–493.

Brenner, H. 1961. The slow viscous motion of a sphere through a fluid toward a plane surface. *Chem. Eng. Sci.* 16:242–251.

Butcher, E., R. Scollay, and I. Weissman. 1980. Organ specificity of lymphocyte migration: mediation by highly selective lymphocyte interaction with organ specific determinants on high endothelial venules. *Eur. J. Immunol.* 10:556–561.

Cozens-Roberts, C., J. A. Quinn, and D. A. Lauffenburger. 1990*a*. Receptor-mediated cell adhesion phenomena. Model studies with the radial-flow detachment assay. *Biophys. J.* 58:107–125.

Cozens-Roberts, C., D. A. Lauffenburger, and J. A. Quinn. 1990*b*. Receptor-mediated cell attachment and detachment. I. Probabilistic model and analysis. *Biophys. J.* 58:841–856.

Cozens-Roberts, C., D. A. Lauffenburger, and J. A. Quinn. 1990*c*. Receptor-mediated cell attachment and detachment. II. Experimental model studies with the radial-flow detachment assay. *Biophys. J.* 58:857–872.

Dembo, M., D. C. Torney, K. Saxman, and D. A. Hammer. 1988. The reaction-limited kinetics of membrane-to-surface adhesion and detachment. *Proc. R. Soc. Lond. B. Biol. Sci.* 234:55–83.

DiMilla, P. A., K. Barbee, and D. A. Lauffenburger. 1991. Mathematical model for the effects of adhesion and mechanics on cell migration speed. *Biophys. J.* 60:15–37.

Doroszewski, J. 1980. Short-term and incomplete cell-substrate adhesion. *In* Cell Adhesion and Motility. A. S. G. Curtis and J. D. Pitts, editors. Cambridge University Press, United Kingdom. 171–197.

Evans, E. A. 1985*a*. Detailed mechanics of membrane–membrane adhesion and separation. I. Continuum of molecular cross-bridges. *Biophys. J.* 48:175–183.

Evans, E. A. 1985*b*. Detailed mechanics of membrane–membrane adhesion and separation. II. Discrete kinetically trapped molecular cross-bridges. *Biophys. J.* 48:185–192.

Evans, E., and A. Yeung. 1989. Apparent viscosity and cortical tension of blood granulocytes determined by micropipet aspiration. *Biophys. J.* 56:151–160.

Evans, E., D. Berk, and A. Leung. 1991. Detachment of agglutinin-bonded red blood cells. I. Forces to rupture molecular point attachments. *Biophys. J.* 59:838–848.

Gardiner, C. W. 1985. Handbook of stochastic methods for physics, chemistry and the natural sciences. Springer-Verlag, Berlin, Germany.

Goldman, A. J., R. G. Cox, and H. Brenner. 1967*a*. Slow viscous motion of a sphere parallel to a plane wall. I. Motion through a quiescent fluid. *Chem. Eng. Sci.* 22:637–652.

Goldman, A. J., R. G. Cox, and H. Brenner. 1967*b*. Slow viscous motion of a sphere parallel to a plane wall: II. Couette Flow. *Chem. Eng. Sci.* 22:653–659.

Hammer, D. A., and D. A. Lauffenburger. 1987. A dynamical model for receptor-mediated cell adhesion to surfaces. *Biophys. J.* 52:475–487.

Hammer, D. A. 1992. Simulation of cell rolling and adhesion on surfaces in shear flow: microvilli-coated hard spheres with adhesive springs, Conference Proceedings for 1991 BMES Meeting, Charlottesville, VA. L. Weiss and K. W. Anderson, editors. *Cell Biophys.* In press.

Harlan, J. M. 1975. Leukocyte-endothelial interactions. *Blood.* 65:513–525.

Helm, C. A., W. Knoll, and J. N. Israelachvili. 1991. Measurement of ligand-receptor interactions. *Proc. Natl. Acad. Sci. USA.* 88:8169–8173.

Hiemenz, P. C. 1986. Principles of colloid and surface chemistry. 2nd Edition. Marcell Dekker, Inc. New York, NY.

House, S. D., and H. H. Lipowsky. 1991. Dynamics of leukocyte-endothelium interactions in the splanchnic microcirculation. *Microvas. Res.* 42:288–304.

Israelachvili, J. N. 1985. Intermolecular and surface forces. With applications to colloidal and biological systems. Academic Press, San Diego, CA.

Jacobson, K., D. O'Dell, and J. T. August. 1984. Lateral diffusion of a 80,000 dalton glycoprotein in the plasma membrane of murine fibroblasts: relationship to structure and function. *J. Cell Biol.* 99:1624–1633.

Jeffrey, G. B. 1915. On the steady rotation of a solid of revolution in a viscous fluid. *Proc. Lond. Math. Soc.* 14:327–338.

Knutton, S., M. C. B. Sumner, and C. A. Pasternak. 1975. Role of microvilli in surface changes of synchronized P815Y mastocytoma cells. *J. Cell Biol.* 66:568–576.

Lawrence, M. B., C. W. Smith, S. G. Eskin, and L. V. McIntire. 1990. Effect of venous shear stress on CD18-mediated neutrophil adhesion to cultured endothelium. *Blood.* 75:227–237.

Lawrence, M. B., and T. A. Springer. 1991. Leukocytes roll on a selectin at physiological flow rates: distinction from and prerequisite for adhesion through integrins. *Cell.* 65:859–874.

Ley, K., P. Gaehtgens, C. Fennie, M. S. Singer, L. A. Lasky, and S. D. Rosen. 1991. Lectin-like cell adhesion molecule 1 mediates leukocyte rolling in mesenteric venules in vivo. *Blood.* 77:2553–2555.

Lipowsky, H. H., D. Riedel, and G. S. Shi. 1991. In vivo mechanical properties of leukocytes during adhesion to venular endothelium. *Biorheology.* 28:53–64.

Loor, F., and L.-B. Hagg. 1975. The modulation of microprojections on the lymphocyte membrane and the redistribution of membrane bound ligands, a correlation. *Eur. J. Immunol.* 6:854–865.

Napper, D. H. 1983. Polymeric stabilization of colloidal dispersions. Academic Press, San Diego, CA.

Northrup, S. H. 1988. Diffusion-controlled ligand binding to multiple competing cell-bound receptors. *J. Phys. Chem.* 92:5847–5850.

Ohshima, H., K. Makino, and T. Kondo. 1987. Electrostatic interaction of two parallel plates with surface charge layers. *J. Colloid Inter. Sci.* 116:196–199.

Pauli, B. U., H. G. Augustin-Voss, M. E. El-Sabban, R. C. Johnson, and D. A. Hammer. 1990. Organ preference of metastasis. The role of endothelial cell adhesion molecules. *Cancer and Metastasis Reviews.* 9:175–189.

Picker, L. J., R. A. Warnock, A. R. Burns, C. M. Doerschuk, E. L. Berg, and E. C. Butcher. 1991. The neutrophil selectin LECAM-1 presents carbohydrate ligands to the vascular selectins ELAM-1 and GMP-140. *Cell.* 66:921–934.

Rice, G. E., and M. P. Bevilacqua. 1989. An inducible endothelial cell surface glycoprotein mediated melanoma adhesion. *Science (Wash. DC).* 246:1303–1306.

Schmid-Schönbein, G. W., R. Skalak, S. I. Simon, and R. L. Engler. 1987. The interaction between leukocytes and endothelium in vivo. *In* Blood Contact with Natural and Artificial Surfaces. *Ann. NY Acad. Sci.* 516:348–361.

Schmidt, E. E., I. C. MacDonald, and A. C. Groom. 1990. Interactions of leukocytes with vessel walls and with other blood cells, studied by high resolution intravital videomicroscopy of spleen. *Microvas. Res.* 40:99–117.

Springer, T. A. 1990. Adhesion receptors of the immune system. *Nature (Lond.).* 346:425–434.

Tempelman, L. A., and D. A. Hammer. 1990. Quantifying receptor-mediated cell adhesion under flow using a model cell line. *J. Cell Biol.* 111:404*a*. (Abstr.)

Tissot, O., C. Foa, C. Capo, H. Brailly, M. Delaage, and P. Bongrand. 1991. Influence of adhesive bonds and surface rigosity on the interaction between rat thymocytes and flat surfaces under laminar shear flow. *J. Dispersion Sci. Tech.* 12:145–160.

Tözeren, A. 1990. Cell–cell, cell-substrate adhesion: theoretical and experimental considerations. *J. Biomech. Eng.* 112:311–318.

von Adrian, U. H., J. D. Chambers, L. M. McEvoy, R. F. Bargatze, K. E. Arfors, and E. C. Butcher. 1991. Two-step model of leukocyte-endothelial cell interaction in inflammation: distinct roles for LECAM-1 and the leukocyte β_2 integrins in vivo. *Proc. Natl. Acad. Sci. USA.* 88:7538–7542.

Wattenbarger, M. R., D. J. Graves, and D. A. Lauffenburger. 1990. Specific adhesion of glycophorin liposomes to a lectin surface in shear flow. *Biophys. J.* 57:765–778.

Weiss, L. 1990. Metastatic inefficiency. *Adv. Can. Res.* 54:159–211.

Yeung, A., and E. Evans. 1989. Cortical shell-liquid core model for passive flow of liquid-like spherical cells into micropipets. *Biophys. J.* 56:139–149.